2005-2017 ozone trends and potential benefits of local measures as deduced from air quality measurements in the north of the Barcelona Metropolitan Area

Jordi Massagué[1, 2], Cristina Carnerero[1, 2], Miguel Escudero[3], José María Baldasano[4], Andrés Alastuey[1], Xavier Querol[1]

[1] Institute of Environmental Assessment and Water Research (IDAEA-CSIC), Barcelona, 08034, Spain.

[2] Department of Civil and Environmental Engineering, Universitat Politècnica de Catalunya, Barcelona, 08034, Spain.

[3] Centro Universitario de la Defensa, Academia General Militar, 50090 Zaragoza, Spain.

[4] Department of Projects and Construction Engineering (DEPC), Universitat Politècnica de Catalunya, 08028 Barcelona, Spain.

Abstract

We analyzed 2005–2017 data sets on ozone (O_3) concentrations in an area (the Vic Plain) frequently affected by the atmospheric plume northward transport of Barcelona Metropolitan Area (BMA), the atmospheric basin of Spain recording the highest number of exceedances of the hourly O_3 information threshold (180 μg m^{-3}). We aimed at evaluating the potential benefits of implementing local-BMA short-term measures to abate emissions of precursors. To this end, we analyzed in detail spatial and time variations of concentration of O_3 and nitrogen oxides (NO and NO_2, including OMI remote sensing data for the latter). Subsequently, a sensitivity analysis is done with the air quality (AQ) data to evaluate potential O_3 reductions in the North of the BMA on Sundays, compared with weekdays as a consequence of the reduction in regional emissions of precursors.

The results showed a generalized decreasing trend for regional background O_3 as well as the well-known increase of urban O_3 and higher urban NO decreasing slopes compared with those of NO_2. The most intensive O_3 episodes in the Vic Plain are caused by (i) a relatively high regional background O_3 (due to a mix of continental, hemispheric–tropospheric and stratospheric contributions); (ii) intensive surface fumigation from mid-troposphere high O_3 upper layers arising from the concatenation of the vertical recirculation of air masses, but also by (iii) an important O_3 contribution from the northward transport/channeling of the pollution plume from the BMA. The high relevance of the local-daily O_3 contribution during the most intense pollution episodes is clearly supported by the O_3 (surface concentration) and NO_2 (OMI data) data analysis.

A maximum decrease potential (by applying short-term measures to abate emissions of O_3 precursors) of 49 μg O_3 m^{-3} (32%) of the average diurnal concentrations was determined. Structurally implemented measures, instead of episodically, could result in important additional O_3 decreases because not only the local O_3 coming from the BMA plume would be reduced but also the recirculated O_3 and thus the intensity of O_3 fumigation in the Plain. Therefore, it is highly probable that both structural and episodic measures to abate NO_x and volatile organic compounds (VOCs) emissions in the BMA would result in evident reductions of O_3 in the Vic Plain.

Keywords: tropospheric ozone, regional pollution, photochemistry, air quality trends.

1. Introduction

Tropospheric ozone (O_3) is a secondary atmospheric pollutant produced by the photooxidation of volatile organic compounds (VOCs) in the presence of nitrogen oxides (NO_x = NO + NO_2). Its generation is enhanced under high temperature and solar radiation (Monks et al., 2015 and references therein). Thus, O_3 maxima occur generally in the afternoon, with the highest levels typically registered in summer, when exceedances of regulatory thresholds are most frequent.

O_3 is one of the key air pollutants affecting human health and the environment (WHO, 2006, 2013a, 2013b; GBD, 2016; Fowler et al., 2009; IPCC, 2013). According to EEA (2018), in the period 2013–2015, more than 95% of the urban population in the EU-28 was exposed to O_3 levels exceeding the WHO guidelines set for the protection of the human health (maximum daily 8-h average concentration of 100 μg m^{-3}).

On a global scale, approximately 90% of the tropospheric O_3 is produced photochemically within the troposphere (Stevenson et al., 2006; Young et al., 2013), the remaining part being transported from the stratosphere (McLinden et al., 2000; Olson et al., 2001). The main global sink of tropospheric O_3 is photolysis in the presence of water vapor. Dry deposition, mainly by vegetation, is also an important sink in the continental planetary boundary layer (PBL) (Jacob and Winner, 2009).

On a regional scale, O_3 levels vary substantially depending on the different chemical environments within the troposphere. O_3 chemical destruction is largest where water vapor concentrations are high, mainly in the lower troposphere, and in polluted areas where there is direct O_3 destruction by titration. Thus, the hourly, daily and annual variations in O_3 levels at a given location are determined by several factors, including the geographical characteristics, the predominant meteorological conditions and the proximity to large sources of O_3 precursors (Logan, 1985).

Southern Europe, especially the Mediterranean basin, is the most exposed to O_3 pollution in Europe (EEA, 2018) due to the specific prevailing meteorological conditions during warm seasons, regional pollutant emissions, high biogenic VOCs' (BVOCs) emissions in spring and summer and the vertical recirculation of air masses due to the particular orographic features that help stagnation–recirculation episodes (Millán et al., 2000; EC, 2002, 2004; Millán, 2009; Diéguez et al., 2009, 2014; Valverde et al., 2016). Periods with high O_3 concentrations often last for several days and can be detected simultaneously in several countries. Lelieveld et al. (2002) reported that during summer, O_3 concentrations are 2.5–3 times higher than in the hemispheric background troposphere. High O_3 levels are common in the area, not only at the surface but also throughout the PBL (Millán et al., 1997; Gangoiti et al., 2001; Kalabokas et al., 2007). Photochemical O_3 production is favored due to frequent anticyclonic conditions with clear skies during summer, causing high insolation and temperatures and low rainfall. Besides, the emissions from the sources located around the basin, which is highly populated and industrialized, and the long-range transport of O_3 contribute to the high concentrations (Millán et al., 2000; Lelieveld et al., 2002; Gerasopoulos, 2005; Safieddine et al., 2014).

In this context, the design of efficient O_3 abatement policies is difficult due to the following circumstances:

- The meteorology driving O_3 dynamics is highly influenced by the complex topography surrounding the basin (see the above references for vertical recirculation of air masses and Mantilla et al., 1997; Salvador et al., 1997; Jiménez and Baldasano, 2004; Stein et al., 2004).
- The complex nonlinear chemical reactions between NO_x and VOCs (Finlayson-Pitts and Pitts, 1993; Pusede et al., 2015), in addition to the vast variety of the VOCs precursors involved and the involvement of BVOCs in O_3 formation and destruction (Hewitt et al., 2011).
- The transboundary transport of air masses containing significant concentrations of O_3 and its precursors, which contribute to increased O_3 levels, mainly background concentrations (UNECE, 2010).
- The contribution from stratospheric intrusions (Kalabokas et al., 2007).
- The fact that O_3 concentrations tend to be higher in rural areas (EEA, 2018), where local mitigation plans are frequently inefficient, because the emission of precursors takes place mostly in distant urban and industrial agglomerations.

Sicard et al. (2013) analyzed O_3 time trends during 2000–2010 in the Mediterranean and observed a slight decrease of annual O_3 averages (–0.4% per year) at rural sites, and an increase at urban and suburban stations (+0.6% and +0.4%, respectively). They attributed the reduction at rural sites to the abatement of NO_x and VOCs emissions in the EU. Paradoxically, this led to an increase in O_3 at urban sites due to a reduction in the titration by NO. Their results also suggested a tendency to converge at remote and urban sites. Paoletti et al. (2014) also reported convergence in the EU and the US in the period 1990–2010 but found increasing annual averages at both rural and urban sites, with a faster increase in urban areas. Querol et al. (2016) determined that O_3 levels in Spain remained constant at rural sites and increased at urban sites in the period 2000–2015. This was suggested to be a result of the preferential reduction of NO versus NO_2, supported by the lack of a clear trend in O_x (O_3 + NO_2). They also found that the target value was constantly exceeded in large areas of the Spanish territory, while most of the exceedances of the information threshold took place in July, mainly downwind of

urban areas and industrial sites, and were highly influenced by summer heatwaves. The Vic Plain (located north of Barcelona) was the area registering the most annual exceedances of the information threshold in Spain, with an average of 15 exceedances per year per site.

In this study, we analyze NO, NO_2 and O_3 surface data around the Barcelona Metropolitan Area (BMA) and the Vic Plain, as well as NO_2 satellite observations, in the period 2005–2017, with the aim of better understanding the occurrence of high O_3 episodes in the area on a long-term basis. Previous studies in this region focused on specific episodes, whereas we aim at assessing the spatial distribution, time trends and temporal patterns of O_3 and its precursors, and the exceedances of the information threshold on a long time series. After better understanding the 2005–2017 O_3 episodes, we aim to evaluate, as a first approximation using air quality monitoring and OMI remote sensing data, the effect that episodic mitigation measures of O_3 precursors would have in the O_x concentrations in the Vic Plain.

We recognize that the O_3 problem has to be studied with executable models with dispersion and photochemical modules, which allow performing sensitivity analyses. It is also well recognized that there is a complex O_3 phenomenology in the study area and that although models have greatly improved in the last 10 years, there are still problems in reproducing some of the processes in detail, such as the channeling of O_3 plumes in narrow valleys or the vertical recirculation patterns. Our study intends to obtain a sensitivity analysis for O_3 concentrations using air quality data. Ongoing collaboration is being stablished with modelers to try to validate model outputs with this experimental sensitivity analysis and then to implement a prediction system for abating efficiently O_3 precursors to reduce O_3 concentrations, for which executable models are the solely tool available.

2. Methodology

2.1. The area of study

The study is set in central Catalonia (Spain), in the north-eastern corner of the Iberian Peninsula (Figure 1). Characterized by a Mediterranean climate, summers are hot and dry with clear skies. In the 21st century, heat waves have occurred frequently in the area, often associated with high O_3 levels (Vautard et al., 2007; Guerova et al., 2007; Querol et al., 2016; Guo et al., 2017).

The capital city, Barcelona, is located on the shoreline of the Mediterranean Sea. Two sets of mountain chains lie parallel to the coastline (SW–NE orientation) and enclose the Pre-coastal Depression: the Coastal (250–500 m above sea level (a.s.l.)) and the Pre-Coastal (1000–1500 m a.s.l.) mountain ranges. The Vic Plain, situated 45–70 km North of Barcelona (500 m a.s.l.) is a 230 km^2 plateau that stretches along a S–N direction and is surrounded by high mountains (over 1000 m a.s.l.). The complex topography of the area protects it from Atlantic advections and continental air masses but also hinders the dispersion of pollutants (Baldasano et al., 1994). The two main rivers in the area (Llobregat and Besòs) flow perpendicularly to the sea and frame the city of Barcelona. Both rivers' valleys play an important role in the creation of air-flow patterns. The Congost River is a tributary to the Besòs River and its valley connects the Vic Plain with the Pre-coastal Depression.

The BMA stretches across the Pre-Coastal and Coastal Depressions and is a densely populated (>1500 people per km^2, MFom, 2017) and highly industrialized area with large emissions originating from road traffic, aircraft, shipping, industries, biomass burning, power generation and livestock.

During summer, the coupling of daily upslope winds and sea breezes may cause the penetration of polluted air masses up to 160 km inland, channeled from the BMA northward by the complex orography of the area. These air masses are injected at high altitudes (2000–3000 m a.s.l.) by the Pyrenean mountain ranges. At night time, the land breeze prevails, and winds flow toward the sea followed by subsidence sinking of the air mass, which can be transported again by the sea breeze of the following day (Millán et al., 1997, 2000, 2002; Toll and Baldasano, 2000; Gangoiti, 2001; Gonçalves et al., 2009; Millán, 2014; Valverde et al., 2016). Under conditions of a lack of large-scale forcing and the development of a thermal low over the Iberian Peninsula that forces the confluence of surface winds from coastal areas toward the central plateau, this vertical recirculation of the air masses results in regional summer O_3 episodes in the Western Mediterranean. In

addition, there might be external O_3 contributions, such as hemispheric transport or stratospheric intrusions (Kalabokas et al., 2007, 2008, 2017; Querol et al., 2017, 2018).

2.2. Air quality, meteorological and remote sensing data

We evaluated O_3 and NO_x AQ data together with meteorological variables and satellite observations of background NO_2.

The regional government of Catalonia (Generalitat de Catalunya, GC) has a monitoring network of stations that provides average hourly data of air pollutants (XVPCA, GC, 2017a, b). We selected a total of 25 stations (see Figure 2). To study the O_3 phenomenology in the Vic Plain, we selected the 8 stations marked in green, which met the following constraints: (i) location along the S–N axis (Barcelona–Vic Plain–Pre-Pyrenean Range); (ii) availability of O_3 measurements; (iii) availability of at least 9 years of data in the period 2005–2017, with at least 75% data coverage from April to September. The remaining selected stations (used only as reference ones for interpreting data from the main Vic-BMA axis stations) met the following criteria: (i) location across the Catalan territory, and (ii) availability of a minimum of 5 years of valid O_3 data in the period 2005–2017. We chose this period due to the poor data coverage of most of the AQ sites in the regional network of AQ monitoring stations before 2005.

In addition, we selected wind and temperature data from 5 meteorological stations from the Network of Automatic Meteorological Stations (XEMA, Meteocat, 2017) closely located to the previously selected AQ stations, as well as solar radiation data from two solar radiation sites from the Catalan Network of Solar Radiation Measurement Stations (ICAEN-UPC, 2018) located in the cities of Girona and Barcelona.

We also used daily tropospheric NO_2 column satellite measurements using the Ozone Monitoring Instrument (OMI) spectrometer aboard NASA's Earth Observing System (EOS) Aura satellite (see OMI, 2012; Krotkov and Veefkind, 2016). The measurements are suitable for all atmospheric conditions and for sky conditions where cloud fraction is less than 30% binned and averaged into $0.25^\circ \times 0.25^\circ$ global grids.

2.3. Data analysis

2.3.1. O_x calculations

We calculated O_x concentrations to better interpret O_3 dynamics. Kley and Gleiss (1994) proposed the concept of O_x to improve the spatial and temporal variability analysis by decreasing the effect of titration of O_3 by NO with the subsequent consumption of O_3 in areas where NO concentrations are high. Concentrations were transformed to ppb units using the conversion factors at 20 °C and 1 atm (DEFRA, 2014).

O_x concentrations were only calculated if there were at least 6 simultaneous hourly recordings of O_3 and NO_2 from 12:00 to 19:00 h, June–August, in the period 2005–2017. The stations used for these calculations were those located along the S–N axis (Barcelona–Vic Plain–Pre-Pyrenean Range).

2.3.2. Variability of concentrations across the air quality monitoring network

To study the variability of concentrations of NO, NO_2, O_3 and O_x across the air quality monitoring network we calculated June–August averages (months recording the highest concentrations of O_3 in the area) from hourly concentrations provided by all the selected AQ sites. For each of them, we calculated daily averages and daytime high averages (12:00 to 19:00 h).

2.3.3. Time trends

By means of the Mann–Kendall method, we analyzed time trends for NO, NO_2 and O_3 for the period 2005–2017. In addition, we used the Theil–Sen statistical estimator (Theil, 1950; Sen, 1968) implemented in the R package Openair (Carslaw and Ropkins, 2012) to obtain the regression parameters of the trends (slope, uncertainty and p-value) estimated via bootstrap resampling. We examined the annual time trends of seasonal averages (April–September) for each pollutant. Data used for these calculations were selected according to the recommendations in EMEP-CCC (2016): the stations considered have at least 10 years of data (75% of the total period considered, 2005–2017) and at least 75% of the data is available within each season. In addition,

we analyzed annual time trends of tropospheric NO_2 measured by satellite along the S–N axis and of greenhouse gases (GHGs) emitted in Catalonia and the average number of vehicles entering the city of Barcelona.

2.3.4. Assessment of O_3 objectives according to air quality standards

We identified the maximum daily 8-hour average concentrations by examining 8-h running averages using hourly data in the period 2005–2017. Each 8-h average was assigned to the day on which it ended (i.e., the first average of one day starts at 17:00 h on the previous day), as determined by EC (2008).

To assess the time trends and patterns of the Exceedances of Hourly Information Thresholds (EHITs) established by EC (2008) (hourly mean of O_3 concentration greater than 180 μg m^{-3}), we used all the data, independently of the percentage of data availability.

2.3.5. Tropospheric NO_2 column

We analyzed daily average Tropospheric Column NO_2 measurements from 2005 to 2017 aiming at two different goals. On the one hand, to quantify the tropospheric NO_2 in the area along the S–N axis and obtain annual time trends and monthly/weekly patterns. On the other hand, to assess qualitatively the tropospheric NO_2 across a regional scale (Western Mediterranean Europe) in two different scenarios, by means of visually finding patterns that might provide a better understanding of O_3 dynamics in our area of study. The scenarios were: days with the maximum 8-h O_3 average above the 75th percentile at the Vic Plain stations, and days with the maximum below the 25th percentile. See selected regions for retrieval of NO_2 satellite measurements in Figure S1.

2.3.6. Time conventions

When expressing average concentrations, the times shown indicate the start time of the average. For example, 12:00–19:00 h averages take into account data registered from 12:00 h to 19:59 h. All times are expressed as local time (UTC + 1 hour during winter and UTC + 2 hours during summer) and the 24-hour time clock convention is used.

3. Results and discussion

3.1. Variability of concentration of pollutants across the air quality monitoring network

We analyzed the mean NO, NO_2, O_3 and O_x concentrations (June to August) in the study area in the period 2005–2017.

As expected, the highest NO and NO_2 concentrations are registered in urban/suburban (U/SU) traffic sites in and around Barcelona (MON, GRA, MNR and CTL, 7–10 μg NO m^{-3} and CTL and MON 30–36 μg NO_2 m^{-3}). Also, as expected, the remote high-altitude rural background (RB) sites (MSY and MSC) register the lowest NO (<1 μg m^{-3}) and NO_2 (2–4 μg m^{-3}) concentrations, see Figure S2.

The lowest June–August average O_3 concentrations (45–60 μg m^{-3}) are recorded in the same U/SU traffic sites (MON, GRA, MNR and CTL) where titration by NO is notable, while the highest ones (>85 μg m^{-3}) are recorded at the RB sites, MSC being the station recording the highest June–August O_3 levels (102 μg m^{-3}). These spatial patterns are significantly different when we consider the 8-h daily averages of O_3 concentrations for June–August 12:00–19:00 h (Figure 3a). Thus, these concentrations are repeatedly high (85–115 μg m^{-3}) in the whole area of study. The highest O_3 concentrations (>107 μgm^{-3}) were recorded at the four sites located downwind of BMA along the S–N corridor (MSY, TON, VIC and MAN), and downwind of Tarragona (PON, RB station). Figure 3a also shows a positive O_3 gradient along the S–N axis (O_3 levels increase farther north) following the BMA plume transport and probably an increase of the mixing layer height (MLH). The higher O_3 production and/or fumigation in the northern areas are further supported by the parallel northward increasing O_x gradient (δO_x Figure 3b). Time series show that in 85% of the valid data in June–August (849 out of 1001 days in 2005–2017) this positive gradient is evident between CTL and TON ($\delta O_{x\,TON\text{-}CTL} > 0$). The average O_x increase between

CTL in Barcelona and TON is 15 ppb. Taking into account the low NO_2 concentrations registered at this station, this is equivalent to approximately 29 μg m^{-3} of O_3 (+30% O_x in TON compared with CTL).

Thus, TON at the Vic Plain records the highest 12:00–19:00 h, June–August O_x and O_3 concentrations in the study area. The MNR site also exhibits very high O_x levels (Figure 3b) but these are mainly caused by primary NO_2 associated with traffic emissions.

3.2. Time patterns

3.2.1. Annual trends

Figure 4 shows the results of the trend analysis of NO, NO_2, O_3 and O_x averages (April to September, the O_3 season according to the European AQ Directive) by means of the Mann–Kendall test.

NO_x levels exhibit a generalized and progressive decrease during the time period across Catalonia. In particular, NO_2 tended to decrease along the S–N axis during the period (U/SU sites CTL, MON and MAN registered –1.6, –2.0 and –1.3% $year^{-1}$, respectively, with statistical significance in all cases). A similar trend was found for NO in these stations, with higher negative slopes (–2.2, –4.3 and –1.1% $year^{-1}$, the latter without statistical significance).

The annual averages of tropospheric NO_2 across the S–N axis decreased by 35% from 2005 to 2017 (–3.4% $year^{-1}$ with statistical significance). The marked drop of NO_2 from 2007–2008 can be attributed to the reduction of emissions associated with the financial crisis starting in 2008. The time trends of average traffic (number of vehicles) entering Barcelona City on working days from 2005 to 2016 (Ajuntament de Barcelona, 2010, 2017) and the GHGs emitted in Catalonia attributed to industry and power generation sectors calculated from the Emissions Inventories published by the Regional Government of Catalonia from 2005 to 2016 (GC, 2017c) (Figure 5a) support this hypothesis. We found both decreasing trends to be statistically significant but the GHG emissions decreasing trend is significantly higher (–3.8% $year^{-1}$) than the traffic (–1.2% $year^{-1}$), which suggests that the crisis had a more severe effect on industry and power generation than on road traffic. This is also supported by a larger decrease of GHG emissions and OMI-NO_2 from 2005–2007 (precrisis) to 2008 (start of the crisis) than BMA traffic counting and urban NO_x levels (without a 2007–2008 steep change and a more progressive decrease, Figure 5b). Thus, in the BMA, the financial crisis caused a more progressive decrease (without a 2007–2008 steep change) of the circulating vehicles and therefore its associated emissions.

April–September O_3 and O_x mean concentration trends are shown in Figure 4. The data show that seven out of the eight RB sites registered slight decreases in O_3 concentrations during the period (BdC, AGU and STP; –1.6% $year^{-1}$, –1.1% $year^{-1}$ and –1.4% $year^{-1}$, respectively, in all cases with statistical significance) while in BEG, PON, LSE and GAN the trends were not significant (not shown). As in several regions of Spain and Europe (Sicard et al., 2013; Paoletti et al., 2014; EEA, 2016; Querol et al., 2016; EMEP, 2016), the opposite trends are found for U/SU sites, with increases in O_3 concentrations during the period at some stations (CTL, MON, MAN, MAT, MNR and ALC; +0.4 to +3.2% $year^{-1}$ all with statistical significance). When considering O_x, the increasing trends in U/SU sites are neutralized in some cases (CTL, MON, MAN, MAT and ALC). This, and the higher NO decreasing slopes compared with those of NO_2, support the hypothesis that the U/SU O_3 increasing trends are probably caused by less O_3 titration (due to decrements in NO levels) instead of a higher O_3 generation. The marked decrease of the vehicle diesel emissions of NO/NO_2 time trends (Carslaw et al., 2016) might have caused this differential NO and NO_2 trends, although other causes cannot be discarded.

3.2.2. Monthly and daily patterns

Figure 6a shows 2005–2017 monthly average hourly O_3 concentrations measured at sites along the S–N axis, showing the occurrence of chronic-type episodes with repeated high O_3 concentrations (90–135 μg m^{-3}) in the afternoon of April–September days at the Vic Plain sites (TON, VIC, MAN) and the remote RB sites (MSY and PAR).

Typically, at the remote RB stations, O_3 concentrations are high during the whole day throughout the year, and daily O_3 variations are narrower than at the other stations, with high average levels even during October–February (MSY: 50–70 and PAR: 50–80 μg m^{-3}). During the night these mountain sites are less affected by NO titration, leading to high daily O_3 average concentrations. However, in summer, midday–afternoon concentrations are relatively lower than at the stations located in the S–N valley (TON, VIC, MAN).

Regarding monthly average daily O_x (Figure 6b), the profiles of RB sites TON and MSY are very similar to the respective O_3 profiles. In the case of the BMA U/SU sites (CTL, MON, GRA), the nocturnal O_x concentrations increase with respect to O_3 due to the addition of secondary NO_2 from titration. Midday–afternoon O_x levels are much lower at the BMA U/SU stations than those in the S–N valley (MAN, TON), similarly to O_3 levels, supporting the contribution of local-regional O_3 from the BMA plume and/or from the fumigation of high-altitude reserve strata as MLH grows (Millán et al., 1997, 2000; Gangoiti et al., 2001; Querol et al., 2017) as well as production of new O_3.

3.2.3. Weekly patterns

Accordingly, Figure 7 shows the O_3 weekly patterns for these O_3 average concentrations. As expected, the variation of intra-annual concentration values is pronounced in the Vic Plain sites (TON, VIC, MAN; 20–45 μg m^{-3} in December–January versus 110–125 μg m^{-3} in July), due to the higher summer photochemistry, the more frequent summer BMA plume transport (due to intense sea breezing) and fumigation from upper atmospheric reservoirs across the S–N axis, and of the high O_3 titration in the populated valleys in winter. However, at the remote mountain sites of MSY and PAR, the intra-annual variability is much reduced (70–80 μg m^{-3} in December versus 100–120 μg m^{-3} in July) probably due to the reduced effect of NO titration at these higher altitude sites, and the influence of high-altitude O_3 regional reservoirs.

During the year, CTL, MON and GRA (U/SU sites around BMA) register very similar weekly patterns of the 8-h maxima, with a marked and typical high O_3 weekend effect, i.e., higher O_3 levels than during the week due to lower NO concentrations. From April to September, CTL O_3 8-h concentrations are lower than MON's and GRA's (the latter located north of BMA following the sea breeze air mass transport), despite being very similar from October to March (when sea breezes are weaker). An O_3 weekend effect is also clearly evident during the winter months in the Vic Plain sites (TON, VIC, MAN) and MSY. However, from June to August, a marked inverse weekend effect is clearly evident at these same sites, with higher O_3 levels during weekdays. This points again to the clear influence of the emission of precursors from the BMA on the O_3 concentrations recorded at these inland sites.

We carried out a trend analysis of NO, NO_2 and O_3 levels measured at AQ sites and background NO_2 from remote sensing (OMI) for weekday (W) and weekend (WE) days independently. To this end we averaged the concentrations for 3 sites in the BMA (CTL, MON and GRA) and 3 receptor sites at the Vic Plain (TON, VIC and MAN), and considering WE to be Saturday, Sunday and Monday for the Vic AQ sites data (adding Mondays to account for the "clean Sunday effect") and Saturday and Sunday for the BMA sites data.

We estimated time trends of W and WE concentrations separately by the Mann-Kendall method along the study period. For O_3 (12:00 to 19:00 h) we found statistically significant increases in both the BMA and the Vic Plain. Increases of O_3 in the BMA double the ones in the Vic Plain and trends of W and WE are very similar per area (O_3 BMA W: +2.0 % $year^{-1}$, O_3 BMA WE: +2.2 % $year^{-1}$, O_3 Vic Plain W: +0.8 % $year^{-1}$, O_3 Vic Plain WE: +1.0 % $year^{-1}$). As seen before, both NO and NO_2 levels (daily averages) in the BMA decrease in a statistically significant way, where NO decrements are larger than NO_2. We found that the decrease of W NO levels is higher than the WE ones (NO BMA W: -3.4 % $year^{-1}$, NO BMA WE: -2.7 % $year^{-1}$) because emissions are higher during W days and these decreased along the period. Regarding NO_2, W and WE decreases remain similar (NO_2 BMA W: -1.9 % $year^{-1}$, NO_2 BMA WE: -1.7 % $year^{-1}$) but lower than NO in both cases thus reducing the O_3 titration effects and increasing O_3 levels both in WE and W days. Regarding NO_2-OMI levels, only W levels show a statistically significant decreasing trend (-3.4 % $year^{-1}$) and not the WE levels.

We then assessed the variations of WE concentrations with respect to W's per year and plotted them by short tilted lines in Figure 8, where the left and right side of each tilted line represent W and WE concentrations respectively. These W to WE variations are then plotted in percentage by continuous lines (>0 depicts increase and <0 decrease W to WE). The upper plot shows O_3 data averaged from 12:00 to 19:00 h from the BMA and the Vic Plain, the middle plot daily averages of NO and NO_2 concentrations in BMA and the bottom plot, daily NO_2-OMI levels along the S-N axis. The results evidence again a constant drop in W to WE NO_x levels in the BMA along the period (negative percentages in the middle plot), with the subsequent O_3 weekend effect in the BMA (positive percentages in the upper plot). In the Vic Plain sites, O_3 concentrations remain constantly high along the study period showing inverse weekend effect almost during the whole period (negative percentages in the plot, except for 2005 to 2007 and 2017). Using the Mann-Kendall test to estimate trends for the W to WE variations we found a clear statistically significant decreasing trend along the period (reduction of the difference between W to WE levels: from -38% in 2005 to -17% in 2017, Figure 8 bottom). We attribute this to the decrease of W-NO_X levels, described before for the annual averages.

Furthermore we found a pattern of nearly parallel O_3 W to WE variation cycles between the Vic Plain and the BMA sites (Figure 8, upper). Due to the inverse W to WE O_3 at Vic and BMA, this parallel trend means in fact that maximum W to WE variations in the Vic Plain and the BMA tend to follow a reverse behavior, i.e. maximum W to WE variations in the BMA tend to occur when W to WE variations in the Vic Plain are minimum (for example 2007, 2010, 2014). NO_x W to WE variations tend to follow a similar behavior than O_3 W to WE variations in the Vic Plain sites (mostly from 2008 to 2016) where years with high W to WE variations of NO_x in the BMA tend to correspond to years with maximum O_3 W to WE variations in the Vic Plain (2009 and 2015). This behavior is probably associated to differences on air mass circulation patterns along the period (such as higher or lower breeze development). Those years with lower breeze development, the transport of the BMA plume is weaker; then NO_x would tend to accumulate at the BMA (low W to WE NO_x variation) which would generate more O_3 thus W to WE variation would be higher in the BMA and lower in the Vic Plain. As opposed, years with stronger breeze development and thus increased transport of the BMA plume, W to WE variations of NO_x in the BMA are higher, W to WE variations of O_3 in the BMA are lower (less O_3 is generated during WE) and higher W to WE O_3 variations are recorded in the Vic Plain sites.

3.3. Peak O_3 concentrations patterns along the S–N axis

July is the month of the year when most of the annual exceedances of the O_3 EHITs are recorded in Spain (Querol et al., 2016), including our area of study. Figure 9 shows the average O_3 and O_x July hourly concentrations along the S–N axis during 2005–2017. A progressive time-shift and a marked positive northward gradient of O_3 and O_x maxima are shown, pointing again to the gradual increase of O_3 and O_x due to the plume transport, new O_3 formation and fumigation from upper reservoirs as MLH grows.

Figure 10a shows the 2005–2017 trends of the EHITs from the European AQ Directive (>180 μg m^{-3} h^{-1} mean; EC, 2008) registered at the selected sites in the S–N valley, as well as the average temperatures measured during July at early afternoon near Vic (at Gurb meteorological site), the background NO_2 measured by OMI (June to August) and the average solar radiation measured in Girona and Barcelona (June to August). In 2005, 2006, 2010, 2013, 2015 and 2017, the highest EHITs at almost all the sites were recorded. Temperature and insolation seem to have a major role in the occurrence of EHITs in 2006, 2010, 2015 and 2017. The effect of heat waves on O_3 episodes is widely known (Solberg et al., 2008; Meehl et al., 2018; Pyrgou et al., 2018; among others). However, because the emissions of precursors have clearly decreased (–30% decrease on June to August OMI-NO_2 levels across the S–N axis from 2005 to 2017; –2.7% $year^{-1}$ with statistical significance) the number of EHITs recorded in the warmest years has probably decreased with respect to a scenario where emissions would have been maintained. In any case, some years (for example 2009 and 2016) seem to be out of line for temperature and insolation being the driving forces, and other major causes also have to be relevant, with further research needed to interpret fully interannual trends. Otero et al. (2016) found that temperature is not the main driver of O_3 in the South-western Mediterranean, as it is in Central Europe, but the O_3 levels recorded the day before (a statistical proxy for the occurrence of Millán et al. (1997)'s vertical

recirculation of air masses). Again, the Vic Plain sites (TON, VIC, MAN) recorded most (75%) of the EHITs reported by the AQ monitoring stations in Catalonia (25%, 34% and 16%, respectively). The higher urban pattern of MAN, as shown by the higher NO concentrations, with respect to TON, might account for both the lower exceedances and the different interannual patterns.

Figure 10b shows that most EHITs occurred in June and July (30% and 57%, respectively), with much less frequency in May, August and September (6%, 8% and <1%, respectively). Although temperatures are higher in August than in June, the latter registers significantly more EHITs, probably due to both the stronger solar radiation and the higher concentrations of precursors (such as NO_2, see OMI-NO_2 and solar radiation in Figure 10b).

Figure 10c shows that EHITs occurred mainly between Tuesday and Friday (average of 19% of occurrences per day). On weekends and Mondays, EHITs were clearly lower (average of 9% of occurrences per day) than during the rest of the week, probably due to: (i) the lower emissions of anthropogenic O_3 precursors (such as NO_x, see OMI-NO_2) during weekends and (ii) to the effect of the lower Sunday emissions in the case of the lower exceedances recorded during Mondays. During weekends and in August, OMI-NO_2 along the S–N axis is relatively lower (–29% weekday average and –43% in August with respect to March) following the emissions patterns associated with industrial and traffic activity that drop during vacations and weekends (Figure 10). NO_x data from AQ monitoring sites follow similar patterns (not shown here).

Figure 10d shows that the frequency of occurrence of the EHITs at MSY (45 km north of Barcelona) is lower and earlier (maxima at 14:00 h) than at Vic Plain sites (TON, VIC, MAN). The EHITs occurred mostly at 15:00, 16:00, 16:00 and 19:00 h at TON, VIC, MAN and PAR (53, 63, 72 and 105 km north of Barcelona), respectively. PAR registered not only much later EHITs, but a much lower number than TON-VIC-MAN sites, again confirming the progressive O_3 maxima time-shift northward of Barcelona.

The results in Figure 11 clearly show that during non-EHIT days, the daily O_3 patterns are governed by the morning–midday concentration growth driven to fumigation and photochemical production, while on EHIT days there is a later abrupt increase, with maxima being delayed as we increase the distance from Barcelona along the S–N axis. This maximal second increase of O_3 is clearly attributable to the influence of the transport of the plume of the BMA (horizontal transport), as the secondary NO_2 peak at 15:00 h (Figure 11 left bottom), and the wind patterns (see Figure S3) seem to support. The differences in the late hourly O_3 concentration increases in EHIT versus non-EHIT days are even more evident when calculating hourly O_3 slopes (hourly increments or decrements of concentrations), Figure 11 (right). The first increment (fumigation and photochemistry) makes O_3 levels scale up to 120 μg m^{-3} during EHIT episodes and to nearly 100 μg m^{-3} during non-EHIT days. In EHIT days, the later peak (transport from BMA and causing most of the 180 μg m^{-3} exceedances) in the O_3 slope occurs again between 14:00 h and 20:00 h, depending on the distance to BMA, but this feature is not observed on non-EHIT days.

3.4. Relevance of local/regional pollution plumes in high O_3 episodes in NE Spain

Figure 12 depicts the basic atmospheric dynamics in the study area during a typical summer day, when the atmospheric conditions are dominated by mesoscale circulations. According to the previous references, indicated in Figure 12 with enclosed numbering (coinciding with the numbering below) the following O_3 contributions to surface concentrations in the study area can be differentiated:

a. Vertical recirculation of O_3-rich air masses, which create reservoir layers of aged pollutants.
b. Vertical fumigation of O_3 from the above reservoirs and the following sources aloft if the MLH growth is large enough:
    b.1. Regional external O_3 layers (from other regions of southern Europe, such as southern France, Italy, Portugal and Tarragona).
    b.2. High free tropospheric O_3 background due to hemispheric long-range transport.
    b.3. High free tropospheric O_3 background due to stratospheric intrusions.

c. Horizontal transport of O_3. Diurnal BMA plume northward transported and channeled into the Besòs–Congost valleys.
d. Local production of O_3 from precursors.

During summer, the intense land heating due to strong solar radiation begins early in the morning. The associated convective activity produces morning fumigation processes (b in Figure 12) that bring down O_3 from the reservoir layers aloft, creating sharp increases in O_3 concentrations in the morning (see Figure 11 and S3). The breeze transports air masses from the sea inland and creates a compensatory subsidence of aged pollutants (including O_3) previously retained in reservoir and external layers and high free troposphere background aloft (Millán et al., 1997, 2000; Gangoiti et al., 2001). This subsided O_3 then affects the marine boundary layer and reaches the city the following day with the sea breeze, producing nearly constant O_3 concentrations in the city during the day (Figure S3 and Figure 9). As the breeze develops, coastal emissions and their photochemical products are transported inland, generating the BMA plume (c in Figure 12) that, in addition to the daily generated O_3, also contains recirculated O_3 from the marine air masses. Furthermore, during the transport to the Vic Plain, new O_3 is produced (d in Figure 12) by the intense solar radiation and the O_3 precursors emitted along the way (e.g., BVOCs from vegetation, NO_x from industrial and urban areas, highways).

This new O_3 gets mixed with the BMA plume and channeled northward to the S–N valleys until it reaches the Vic Plain and the southern slopes of the Pre-Pyrenees. As the BMA plume (loaded with O_3 and precursors) travels northward, a second increase in O_3 concentrations can be observed in the daily cycles of O_3 at these sites, (see Figure 11 and S3). This was described as the second O_3 peak by Millán et al. (2000).

The marked MLH increase in the Vic Plain compared with BMA (Soriano et al., 2001; Querol et al., 2017) may produce a preferential and intensive top-down O_3 transport (b in Figure 12) from upper O_3 layers (a, b.1, b.2 and b.3 in Figure 12), contributing to high O_3 surface concentrations. During the sea/mountain breezes' development, some air masses are injected upward to the N and NW return flows (controlled by the synoptic circulations dominated by the high-pressure system over the Azores) aloft helped by the orography (e.g., southern slopes of mountains) and again transported back to the coastal areas where, at late evening/night it can accumulate at certain altitudes in stably stratified layers.

Later, at night, land breezes returning to the coastal areas develop. Depending on the orography, these drainage flows of colder air traveling to the coastal areas can accumulate on the surface or keep flowing to the sea. The transported O_3 is consumed along the course of the drainage flows by deposition and titration. Next day, the cycle starts anew, producing almost closed loops enhancing O_3 concentrations throughout the days in the area. When the loop is active for several days, multiple O_3 EHITs occur over the Vic Plain.

The main complexity of this system arises from the fact that all these vertical/horizontal, local/regional/hemispheric/stratospheric contributions are mixed and all contribute to surface O_3 concentrations with different proportions that may largely vary with time and space across the study area. However, for the most intense O_3 episodes, the local-regional contribution might be very relevant to cause EHITs in the region. Furthermore, the intensity and frequency of O_3 episodes are partially driven by the occurrence of heat waves in summer and spring (Vautard et al., 2007; Gerova et al., 2007; Querol et al., 2016; Guo et al., 2017). If local and regional emissions of precursors are high, the intensity of the episodes will also be high. Thus, even though heat wave occurrences increase the severity of O_3 episodes, an effort to reduce precursors should be undertaken to decrease their intensity.

The generation of the O_3 episodes in 2005–2017 for the S–N corridor BMA–Vic Plain–Pre-Pyrenees occurs in atmospheric scenarios described in detail by Millán et al. (1997, 2000, 2002), Gangoiti et al. (2001), Kalabokas et al. (2007, 2008, 2017), Millán (2014) and Querol et al. (2018) for other regions of the Mediterranean basin, including Spain, or described in the same area for specific episodes (Toll and Baldasano, 2000; Gonçalves et al., 2009; Valverde et al., 2016; Querol et al., 2017). However, results from our study evidence a higher role of

the local-regional emissions on the occurrence of O_3 EHITs. Thus, our results demonstrate an increase in the EHITs northward from Barcelona to around 70 km and a decrease from there to 100 km from Barcelona following the same direction. There is also a higher frequency of occurrence of these in July (and June) and from Tuesday to Friday and a time-shift of the frequency of occurrence of EHITs from 45 to 100 km. The mountain site of MSY (located at 700 m a.s.l.) registered many fewer EHITs than the sites in the valleys (TON-VIC-MAN, 460–600 m a.s.l.) during the period, showing the key role of the valley channeling of the high O_3 and precursors BMA plume in July (when sea breeze and insolation are more intense). Furthermore, at the Vic Plain, we detected an inverse O_3 weekend effect, suggesting that local/regional anthropogenic emissions of precursors play a key role in increasing the number of EHITs on working days, with a Friday/Sunday rate of 5 for VIC for 2005–2017. Despite this clear influence of the BMA plume on EHITs' occurrence, Querol et al. (2017) demonstrated that at high atmospheric altitudes (2000–3000 m a.s.l.) high O_3 concentrations are recorded, in many cases reaching 150 μg m^{-3} due to the frequent occurrence of reservoir strata. As also described above, the higher growth of the MLH in TON-VIC-MAN as compared with the coastal area accounts also for higher top-down O_3 contributions. On the other side, close to the Pyrenees (PAR station), large forested and more humid areas give rise to a thinner MLH, hindering O_3 fumigation too. Furthermore, in these more distant northern regions O_3 consumption by ozonolysis of BVOCs might prevail over production due to weaker solar radiation during the later afternoon.

Figure 13 shows the distribution of average background OMI-NO_2 levels across the Western Mediterranean Basin in two different scenarios: when the O_3 levels in the Vic Plain are low (left) or high (right). To this end, we averaged the values from VIC and TON (in the Vic Plain) from all the maximum daily 8-h mean O_3 concentrations calculated for all the days in July within 2005–2017, and we calculated the 25th (93 out of 370 days, 105 μg m^{-3}) and 75th (93 days, 139.5 μg m^{-3}) percentiles of all the data (P25 and P75, respectively). For both scenarios, NO_2 concentrations are highest around large urban and industrial areas, including Madrid, Porto, Lisbon, Barcelona, Valencia, Paris, Frankfurt, Marseille and especially the Po Valley. The shipping routes toward the Gibraltar Strait and around the Mediterranean can be observed, as well as important highways such as those connecting Barcelona to France and Lyon to Marseille. As expected, the mountain regions (the Pyrenees and the Alps) are the areas with lower NO_2. Regional levels of background OMI-NO_2 in the P75 scenario are markedly higher with hotspots intensified and spanning over broader areas. Over Spain, new hotspots (marked in yellow), such as the coal-fired power plants in Asturias (a), ceramic industries in Castelló (c) and the coal-fired power plant in Andorra, Teruel (b), appear; in the latter case, with the pollution plume being channeled along the Ebro Valley with a NW transport. Furthermore, it is important to highlight that the maxima background NO_2 along the eastern coastline in Spain, including the BMA, tend to exhibit some north-northwest displacement, when compared with the P25 scenario, thus pointing to the relevance of the local emissions in causing inland O_3 episodes.

These qualitative results suggest in general less synoptic forcing in Western Europe in the P75 scenario; hence, in these conditions NO_2 is accumulated across the region and especially around its sources. In the east coast of the Iberian Peninsula, mesoscale circulations tend to dominate, hence the northwest displacement (taking the coastal regions as a reference) of the background NO_2. The bottom part of Figure 13 zooms our study area and shows the maximum daily 8-h mean O_3 concentrations in all the selected AQ sites averaged for both scenarios. As shown in the P75 scenario, NO_2 is significantly intensified across Catalonia, especially north of the BMA spreading to the Vic Plain. Comparing O_3 in both scenarios, in the P75 the O_3 levels are much higher (mostly >105 μg m^{-3}), across the region except the urban sites in Barcelona (due to NO titration), reaching up to 154 μg m^{-3} in the Vic Plain.

Conversely, in the P25 scenario, background NO_2 concentrations are lower, the BMA NO_2 spot is significantly smaller and spreads along the coastline rather than being displaced to the north-northwest. In this case, synoptic flows seem to weaken sea breeze circulations and vertical recirculation, thus reducing the amount of background NO_2 and the inland transport from the coast. In these conditions, O_3 levels are markedly lower across the territory, the RB PON site (downwind of the city/industrial area of Tarragona) being the one recording the maximum daily 8-h mean O_3 concentration (99 μg m^{-3}).

3.5. Sensitivity analysis for O_x using air quality monitoring data

We demonstrated above that the lower anthropogenic emissions of O_3 precursors in the BMA during weekends cause lower O_3 and O_x levels in the Vic Plain than during working days (inverse O_3 weekend effect). To apply a sensitivity analysis using air quality monitoring data for the O_3 levels in the Vic Plain if BMA's emissions were reduced, we compared weekend O_3 and O_x patterns with weekdays considering only data from June and July (August OMI-NO_2 levels are markedly lower, Figure 10b, therefore this month was not included).

Figure 14 shows the average O_x concentrations (12:00 to 19:00 h) in TON and MAN (both AQ sites in the Vic Plain) according to the day of the week for the period considered. Data in VIC cannot be used for O_x calculations due to the lack of NO_2 measurements. Despite the large variability in extreme values (i.e., maximum values with respect to minimum values, represented by whiskers), the interquartile range is quite constant on all the weekdays (between 13.6 to 17.3 ppb in TON and 12.7 to 19.1 in MAN). The average O_x decrease between the day with highest O_x levels (Wednesday in TON and Friday in MAN) and the day with the lowest O_x levels (Sunday in TON and Monday in MAN) is between 6.5 (TON) and 7.7 ppb (MAN) , approximately 13 and 15 μg O_3 m^{-3}, 10-12% decrease). The observed decrements on O_X levels downwind BMA due to the reduction in O_3 precursors' emissions in the BMA during weekends, can give us a first approximation of the effect that episodic mitigation measures could have on the O_X or O_3 levels in the Vic Plain. Thus, we considered feasible a scenario with a maximum potential of O_X reduction of 24.5 ppb (approximately 49 μg O_3 m^{-3}, 32% decrease) when applying episodic mitigation measures (lasting 1-2 days equivalent to a weekend when, on average, NO and NO_2 are reduced 51 and 21%, respectively, compared with week days in the BMA monitoring sites). This was calculated as the difference between the P75 of O_X values observed on Wednesdays minus the P25 of O_x values on Sundays. Obviously, if these mitigation measures would be implemented structurally, instead of episodically, O_x and O_3 decreases would be probably larger because not only the local O_3 coming from the BMA plume would be reduced but also the recirculated O_3 and thus the intensity of O_3 fumigation in the Plain. Therefore, it is probable that both structural and episodic measures to abate VOCs and NO_x emissions in the BMA would result in evident reductions of O_3 in the Vic Plain, as evidenced by modeling tools by Valverde et al. (2016).

4. Conclusions

We analyzed 2005–2017 data sets on ozone (O_3) concentrations in an area frequently affected by the northward atmospheric plume transport of Barcelona Metropolitan Area (BMA) to the Vic Plain, the area of Spain recording the highest number of exceedances of the hourly O_3 information threshold (EHIT, 180 μg m^{-3}). We aimed at evaluating the potential benefits of implementing local short-term measures to abate emissions of precursors. To this end, we analyzed in detail spatial and time (interannual, weekly, daily and hourly) variations of the concentration of O_3 and nitrogen oxides (including remote sensing data for the latter) in April–September and built a conceptual model for the occurrence of high O_3 episodes. Finally, a sensitivity analysis is done with the AQ data to evaluate potential O_3 reductions in the North of the BMA on Sundays, compared with weekdays, as a consequence of the reduction of emissions of precursors.

Results showed a generalized decrease trend for regional background O_3 ranging from –1.1 to –1.6% $year^{-1}$, as well as the well-known increase of urban O_3 (+0.4 to +3.2% $year^{-1}$) and higher urban NO decreasing slopes than those of NO_2 (–2.2 to –4.3 and –1.3 to –2.0% $year^{-1}$, respectively), that might account in part for the urban O_3 increase.

The most intensive O_3 episodes in the North of the BMA have O_3 contributions from relatively high regional background O_3 (due to a mix of continental, hemispheric–tropospheric and stratospheric contributions) as well as O_3 surface fumigation from the mid-troposphere high O_3 upper layers arising from the concatenation of the vertical recirculation of air masses (as a result of the interaction of a complex topography with intensive spring–summer sea and mountain breezes circulations (Millán et al., 1997, 2000; Gangoiti et al., 2001; Valverde et al., 2016; Querol et al., 2017). However, we noticed that for most EHIT days in the Vic Plain, the exceedance occurs when an additional contribution is added to the previous two: O_3 supply by the channeling of the BMA pollution plume along the S–N valley connecting BMA and Vic. Thus, despite the large external O_3

contributions, structural and short-time local measures to abate emissions of precursors might clearly influence spring–summer O_3 in the Vic Plain. This is supported by (i) the reduced hourly exceedances of the O_3 information threshold recorded on Sundays at the Vic AQ monitoring site (9 in 2005–2017) compared with those on Fridays (47), as well as by (ii) the occurrence of a typical and marked Sunday O_3 pattern at the BMA AQ monitoring sites and an also marked but opposite one in the sites of the Vic Plain; and (iii) marked increase of remote sensing OMI-NO_2 concentrations over the BMA and northern regions during days of the P75 diurnal O_3 concentrations compared with those of the P25.

Finally, we calculated the difference between the P75 of O_x diurnal concentrations recorded at two of the Vic Plain AQ monitoring stations for Wednesdays minus those of the P25 percentile of O_x for Sundays, equivalent to 1–2 days of emissions reductions in the BMA. A maximum decrease potential by applying short-term measures of 24.5 ppb (approximately 49 μg O_3 m^{-3}, 32% decrease) of the diurnal concentrations was calculated. Obviously, structurally implemented measures, instead of episodic ones, would result probably in important additional O_x and O_3 abatements because not only the local O_3 coming from the BMA plume would be reduced but also the recirculated O_3, and thus the intensity of O_3 fumigation on the Plain. Therefore, it is highly probable that both structural and episodic measures to abate NO_x and VOCs emissions in the BMA would result in evident reductions of O_3 in the Vic Plain.

Author contributions

JM performed the data compilation, treatment and analysis with the aid of XQ, CC and ME. JM, CC, ME, JB, AA and XQ contributed to the discussion and interpretation of the results. JM and XQ wrote the manuscript. JM, CC, ME, JB, AA and XQ commented on the manuscript.

Competing interests

The authors declare that there is no conflict of interest.

5. Acknowledgments

The present work was supported by the “Agencia Estatal de Investigación” from the Spanish Ministry of Science, Innovation and Universities and FEDER funds under the project HOUSE (CGL2016-78594-R), by the Spanish Ministerio para la Transición Ecológica (17CAES010/ Encargo) and by the Generalitat de Catalunya (AGAUR 2017 SGR41). We would like to thank the Department of Territory and Sustainability of the Generalitat de Catalunya for providing us with air quality data, and the Met Office from Catalonia (Meteocat) for providing meteorological data, as well as to NASA for providing OMI-NO_2 data and the ICAEN-UPC for providing solar radiation measurements. Cristina Carnerero thanks “Agencia Estatal de Investigación” for the Grant received to carry out her Ph.D. (FPI grant: BES-2017-080027).

6. References

Ajuntament de Barcelona: Statistical yearbook of Barcelona City, Year 2010, Statistics department, Barcelona City Council, https://bcnroc.ajuntament.barcelona.cat/jspui/handle/11703/91953, last access: 13 April 2018, 2010.

Ajuntament de Barcelona: Statistical yearbook of Barcelona City, Year 2017, Statistics department, Barcelona City Council, https://bcnroc.ajuntament.barcelona.cat/jspui/handle/11703/106244, last access: 13 April 2018, 2017.

Baldasano, J. M., Cremades, L., and Soriano, C.: Circulation of Air Pollutants over the Barcelona Geographical Area in Summertime, in G. Angeletti and G. Restelli (eds.), Proceedings of the Sixth European Symposium on Physico-Chemical Behavior of Atmospheric Pollutants, Environmental Research Program of the European Community, Air Pollution Research Report EUR 15609/1, 474–479, 1994.

607 Carslaw, D. C. and Ropkins, K.: Openair - an R package for air quality data analysis, Environmental Modelling &
608 Software, Volume 27-28, 52-61, 2012.

609 Carslaw, D. C., Murrells, T.P., Andersson, J., Keenan, M.: Have vehicle emissions of primary NO2 peaked?,
610 Faraday Discussions, Volume 189, 439-454, https://doi.org/10.1039/C5FD00162E, 2016.

611 DEFRA: Department for Environment Food & Rural Affaris, Conversion Factors Between ppb and µgm-3 and
612 ppm and mgm-3, https://uk-
613 air.defra.gov.uk/assets/documents/reports/cat06/0502160851_Conversion_Factors_Between_ppb_and.pdf,
614 last access: 11 February 2018, 2014.

615 Dieguez J.J., Millán M., Padilla L., Palau J.L.: Estudio y evaluación de la contaminación atmosférica por ozono
616 troposférico en España, CEAM Report for the Ministry of Agriculture, Food and Environment, INF FIN/O3/2009,
617 372 pp., 2009.

618 Dieguez J.J., Calatayud V., Mantilla E.: CEAM Report for the Ministry of Agriculture, Food and Environment,
619 Fundación Biodiversidad, Informe Final, Memoria Técnica Proyecto CONOZE, CONtaminación por OZono en
620 España, 137 pp., 2014.

621 EC: Ozone dynamics in the Mediterranean Basin: A collection of scientific papers resulting from the MECAPIP,
622 RECAPMA and SECAP Projects, Air Pollution Report 78, DG RTD I.2, LX 46 2/82, B-1049 Brussels, 2002.

623 EC: European Commission Decision of 19 March 2004 "Concerning guidance for implementation of Directive
624 2002/3/EC of the European Parliament and the Council relating to ozone in ambient air (2004/279/EC), Official
625 Journal of the European Union L87/50 of 25.3.2004, 2004.

626 EC: Directive 2008/50/EC of 21 May 2008. On ambient air quality and cleaner air for Europe, Off. J. Eur. Union,
627 11.6.2008, L152/1, http://eur-lex.europa.eu/legal-content/ES/TXT/?uri=CELEX:32008L0050, last access: 14
628 December 2017, 2008.

629 EEA: Air quality in Europe – 2015 report, EEA Report, No 5/2015 (ISSN 1977-8449), 57 pp., 2015.

630 EEA: Air quality in Europe – 2016 report, EEA Report, No 28/2016 (ISSN 1977-8449), 83 pp., 2016.

631 EEA: Air quality in Europe – 2018 report, EEA Report, No 12/2018 (ISSN 1977-8449), 88 pp., 2018.

632 EMEP-CCC: Air pollution trends in the EMEP region between 1990 and 2012, EMEPCCC-Report 2016/1 102 pp.,
633 http://icpvegetation.ceh.ac.uk/publications/documents/EMEP_Trends_Report_final_published.pdf, last
634 access: 23 January 2018, 2016.

635 Finlayson-Pitts, B.J. and Pitts Jr., J.N.: Atmospheric chemistry of tropospheric ozone formation: scientific and
636 regulatory implications, Air Waste 43 (8), 1091–1100, https://doi.org/10.1080/1073161X.1993.10467187,
637 1993.

638 Fowler, D., Pilegaard, K., Sutton, M. A., Ambus, P., Raivonen, M., Duyzer, J., Simpson, D., Fagerli, H., Fuzzi, S.,
639 Schjoerring, J. K., Granier, C., Neftel, A., Isaksen, I. S. A., Laj, P., Maione, M., Monks, P. S., Burkhardt, J.,
640 Daemmgen, U., Neirynck, J., Personne, E., Wichink-Kruit, R., Butterbach-Bahl, K., Flechard, C., Tuovinen, J. P.,
641 Coyle, M., Gerosa, G., Loubet, B., Altimir, N., Gruenhage, L., Ammann, C., Cieslik, S., Paoletti, E., Mikkelsen, T.
642 N., Ro-Poulsen, H., Cellier, P., Cape, J. N., Horvath, L., Loreto, F., Niinemets, U., Palmer, P. I., Rinne, J., Misztal,
643 P., Nemitz, E., Nilsson, D., Pryor, S., Gallagher, M. W., Vesala, T., Skiba, U., Brueggemann, N., Zechmeister-
644 Boltenstern, S., Williams, J., O'Dowd, C., Facchini, M. C., de Leeuw, G., Flossman, A., Chaumerliac, N., and
645 Erisman, J. W.: Atmospheric composition change: Ecosystems-Atmosphere interactions, Atmospheric
646 Environment, 43, 5193–5267, https://doi.org/10.1016/j.atmosenv.2009.07.068, 2009.

647 Gangoiti G., Millán M.M., Salvador R., and Mantilla E.: Long-range transport and re-circulation of pollutants in
648 the western Mediterranean during the project Regional Cycles of Air Pollution in the West-Central
649 Mediterranean Area, Atmospheric Environment, 35, 6267-6276, https://doi.org/10.1016/S1352-
650 2310(01)00440-X, 2001.

651 GBD: Global Burden of Disease Study 2016 Cause-Specific Mortality 1980-2016, Seattle, United States:
652 Institute for Health Metrics and Evaluation (IHME), 2016.

653 GC: Geoinformation Air Quality information, Departament de Territori I sostenibilitat, Generalitat de
654 Catalunya, http://dtes.gencat.cat/icqa/start.do?lang=en, last access: 23 February 2018, 2017a.

655 GC: Zones de qualitat de l'aire (ZQA), Departament de Territori I sostenibilitat, Generalitat de Catalunya,
656 http://mediambient.gencat.cat/web/.content/home/ambits_dactuacio/atmosfera/qualitat_de_laire/avaluac
657 io/xarxa_de_vigilancia_i_previsio_de_la_contaminacio_atmosferica__xvpca/ZQA/Llista-de-relacio-de-
658 municipis-i-ZQA.PDF, last access: 23 January 2018, 2017b.

659 GC: Catalonia GHG Emissions. Catalan Office of Climate Change, Generalitat de Catalunya,
660 http://canviclimatic.gencat.cat/ca/politiques/inventaris_d_emissions_de_geh/emissions_de_geh_a_catalun
661 ya/, last access: 13 February 2018, 2017c.

662 Gerasopoulos, E., Kouvarakis, G., Vrekoussis, M., Kanakidou, M.,and Mihalopoulos, N.: Ozone variability in the
663 marine boundary layer of the Eastern Mediterranean based on 7-year observations, J. Geophys. Res., 110,
664 D15309, https://doi.org/10.1029/2005JD005991, 2005.

665 Gonçalves M., Jiménez-Guerrero P., and Baldasano J.M.: Contribution of atmospheric processes affecting the
666 dynamics of air pollution in South-Western Europe during a typical summertime photochemical episode,
667 Atmospheric Chemistry and Physics, 9, 849-864, 2009.

668 Guerova, G., Jones, N.: A global model study of ozone distributions during the August 2003 heat wave in
669 Europe, Environmental Chemistry, 4, 285–292, 2007.

670 Guo, Y., Gasparrini, A., Armstrong, B.G., Tawatsupa, B., Tobias, A., Lavigne, E., de Sousa Zanotti Stagliorio
671 Coelho, M., Pan X., Kim H., Hashizume M., Honda Y., Guo Y.-L. L. , Wu Ch-F., Zanobetti A., Schwartz J.D. , Bell
672 M.L., Scortichini M., Michelozzi P., Punnasiri K., Li S., Tian L., Osorio Garcia S.D., Seposo X., Overcenco A., Zeka
673 A., Goodman P., Dang T.N., Dung D.V., Mayvaneh F., Saldiva P.H.N., Williams G., Tong S.: Temperature
674 variability and mortality: a multi-country study, Environmental Health Perspectives 124, 1554, 2016.

675 Hewitt, C. N., Ashworth, K., Boynard, A., Guenther, A., Langford, B., MacKenzie, A. R., Misztal, P. K., Nemitz, E.,
676 Owen, S. M., Possell, M., Pugh, T. A. M., Ryan, A. C., and Wild, O.: Groundlevel ozone influenced by circadian
677 control of isoprene emissions, Nature Geoscience, 4, 671–674, https://doi.org/10.1038/ngeo1271, 2011.

678 ICAEN-UPC: Xarxa de Mesura de la Irradiància Solar a Catalunya, 2018.

679 IPCC: Climate Change 2013, The Physical Science Basis, Working Group I Contribution to the Fifth Assessment
680 Report of the Intergovernmental Panel on Climate Change, edited by: Stocker T.F., Qin D., Plattner G.-K., Tignor
681 M.M.B., Allen S.K., Boschung J., Nauels A., Xia Y., Bex V., Midgley P.M., Cambridge University Press, Cambridge,
682 United Kingdom and New York, NY, USA. http://www.ipcc.ch/report/ar5/wg1/, last access: 23 January 2018,
683 2013.

684 Jacob, D., Winner, D.: Effect of climate change on air quality, Atmospheric Environment 43(1): 51-63,
685 http://nrs.harvard.edu/urn-3:HUL.InstRepos:3553961, last access: 23 January 2018, 2009.

686 Jiménez, P. and Baldasano, J.M.: Ozone response to precursor controls in very complex terrains: use of
687 photochemical indicators to assess O3-NOx-VOC sensitivity in the northeastern Iberian Peninsula, Journal of
688 Geophysical Research 109, D20309, https://doi.org/10.1029/2004JD00498, 2004.

689 Kalabokas, P.D., Volz-Thomas, A., Brioude, J., Thouret, V., Cammas, J.-P., and Repapis, C. C.: Vertical ozone
690 measurements in the troposphere over the Eastern Mediterranean and comparison with Central Europe,
691 Atmospheric Chemistry and Physics, 7, 3783–3790, https://doi.org/10.5194/acp-7-3783-2007, 2007.

692 Kalabokas P.D., Mihalopoulos N., Ellul R., Kleanthous S., Repapis C.C: An investigation of the meteorological
693 and photochemical factors influencing the background rural and marine surface ozone levels in the Central
694 and Eastern Mediterranean, Atmospheric Environment, 42, 7894-7906, 2008.

695 Kalabokas P.D., Hjorth J., Foret G., Dufour G., Eremenko M., Siour G., Cuesta J., Beekmann M.: An investigation
696 on the origin of regional springtime ozone episodes in the western Mediterranean, Atmos. Chem. Phys. 17,
697 3905–3928, 2017.

698 Kley, D. and Geiss, H.: Tropospheric ozone at elevated sites and precursor emissions in the United States and
699 Europe, Atmospheric Environment, 8, 149–158, 1994.

700 Krotkov, N. and Veefkind, P.: OMI/Aura Nitrogen Dioxide (NO2) Total and Tropospheric Column 1-orbit L2
701 Swath 13x24 km V003, Greenbelt, MD, USA, Goddard Earth Sciences Data and Information Services Center
702 (GES DISC), https://doi.org/10.5067/Aura/OMI/DATA2017, 2016.

703 Lelieveld J., Berresheim H., Borrmann S., Crutzen P.J., Dentener F.J., Fischer H., Feichter J., Flatau P.J., Heland
704 J., Holzinger R., Korrmann R., Lawrence M.G., Levin Z., Markowicz K.M., Mihalopoulos N., Minikin A.,
705 Ramanathan V., de Reus M., Roelofs G.J., Scheeren H.A., Sciare J., Schlager H., Schultz M., Siegmund P., Steil
706 B., Stephanou E.G., Stier P., Traub M., Warneke C., Williams J., Ziereis H.: Global air pollution crossroads over
707 the Mediterranean, Science, 298, 794-799, 2002.

708 Logan, J. A.: Tropospheric ozone – seasonal behaviour, trends, and anthropogenic influence, Journal of
709 Geophysical Research: Atmospheres, 90, 10463– 10482, 1985.

710 Mantilla E., Millán M.M., Sanz M.J., Salvador R., and Carratalá A.: Influence of mesometeorological processes
711 on the evolution of ozone levels registered in the Valencian Community, In: I Technical workshop on ozone
712 pollution in southern Europe, Valencia, 1997.

713 McLinden, C. A., Olsen, S. C., Hannegan, B., Wild, O., Prather, M. J., and Sundet, J.: Stratospheric ozone in 3-D
714 models: A simple chemistry and the cross-tropopause flux, Journal of Geophysical Research: Atmospheres,
715 105, 14653–14665, https://doi.org/10.1029/2000jd900124, 2000.

716 Meehl G.A., Tebaldi C., Tilmes S., Lamarque J.F., Bates S.: Future heat waves and surface ozone, Environmental
717 Research Letters 13 064004, https://doi.org/10.1088/1748-9326/aabcdc, 2018.

718 Meteocat: Meteorological Office of Catalonia, Request of meteorological data reports,
719 http://www.meteo.cat/wpweb/serveis/peticions-de-dades/peticio-dinformes-meteorologics/, last access: 23
720 January 2018) and http://meteocat.gencat.cat/observacions/llistat-xema, last access: 6 December 2017, 2017.

721 MFom: Ministerio de Fomento: Áreas urbanas en España 2017, Dirección General de Arquitectura, Vivienda y
722 Suelo, http://atlasau.fomento.gob.es, last access: 6 December 2017, 2017.

723 Millán M.M.: El ozono troposférico en el sur de Europa: aspectos dinámicos documentados en proyectos
724 europeos, CEAM Report for the Ministry of Agriculture, Food and Environment, INF FIN/O3/2009(annex), 156
725 pp., http://www.mapama.gob.es/es/calidad-y-evaluacion-ambiental/temas/atmosfera-y-calidad-del-

aire/Ozono%20Troposf%C3%A9rico%20en%20el%20sur%20de%20Europa-Actualizacion-2009_tcm30-187999.pdf, last access: 13 February 2018, 2009.

Millán M.M.: Extreme hydrometeorological events and climate change predictions in Europe, J. Hydrol. 518B, 206-224, 2014.

Millán M.M., Salvador R., Mantilla E., and Kallos G.: Photooxidant dynamics in the Mediterranean basin in summer: Results from European research projects, Journal of Geophysical Research 102, 8811-8823, 1997.

Millán M.M., Mantilla E., Salvador R., Carratalá A., Sanz M.J., Alonso L., Gangoiti G., and Navazo M.: Ozone Cycles in the Western Mediterranean Basin: Interpretation of Monitoring Data in Complex Coastal Terrain, Journal of Applied Meteorology, 39: 487-508, 2000.

Millán M.M., Sanz M.J., Salvador R., and Mantilla E.: Atmospheric dynamics and ozone cycles related to nitrogen deposition in the western Mediterranean. Environmental Pollution, 118, 167-186, 2002.

Monks P.S., Archibald A.T., Colette A., Cooper O., Coyle M., Derwent R., Fowler D., Granier C., Law K.S., Mills G.E., Stevenson D.S., Tarasova O., Thouret V., von Schneidemesser E., Sommariva R., Wild O., Williams M.L.: Tropospheric ozone and its precursors from the urban to the global scale from air quality to short-lived climate forcer, Atmospheric Chemistry and Physics, 15, 8889-8973, 2015.

Olson, J. R., Crawford, J. H., Davis, D. D., Chen, G., Avery, M. A., Barrick, J. D. W., Sachse, G. W., Vay, S. A., Sandholm, S. T., Tan, D., Brune, W. H., Faloona, I. C., Heikes, B. G., Shetter, R. E., Lefer, B. L., Singh, H. B., Talbot, R. W., and Blake, D. R.: Seasonal differences in the photochemistry of the South Pacific: A comparison of observations and model results from PEM-Tropics A and B, Journal of Geophysical Research, 106, 32749–32766, 2001.

OMI Team: Ozone Monitoring Instrument (OMI) Data User's Guide, https://docserver.gesdisc.eosdis.nasa.gov/repository/Mission/OMI/3.3_ScienceDataProductDocumentation/3.3.2_ProductRequirements_Designs/README.OMI_DUG.pdf, last access: 2 January 2018, 2012.

Otero N., Sillmann J., Schnell J. L., Rust H.W., Butler T.: Synoptic and meteorological drivers of extreme ozone concentrations over Europe, Environ. Res. Lett., 11, 24005, https://doi.org/10.1088/1748-9326/11/2/024005, 2016.

Paoletti, E., De Marco, A., Beddows, D. C. S., Harrison, R. M., & Manning, W. J.: Ozone levels in European and USA cities are increasing more than at rural sites, while peak values are decreasing, Environmental Pollution, 192(x), 295–299, https://doi.org/10.1016/j.envpol.2014.04.040, 2014.

Pay, M. T., Gangoiti, G., Guevara, M., Napelenok, S., Querol, X., Jorba, O., Pérez García-Pando, C.: Ozone source apportionment during peak summer events over southwestern Europe, Atmospheric Chemistry and Physics Discussions, 2018, 1-43, https://doi.org/10.5194/acp-2018-727, 2018.

Pusede, S. E., Steiner, A.L., Cohen, R.C.: Temperature and recent trends in the chemistry of continental surface ozone, Chemical Reviews, 115, 3898–3918, 2015.

Pyrgou A., Hadjinicolaou P., Santamouris M.: Enhanced near-surface ozone under heatwave conditions in a Mediterranean island, Scientific Reports 8, 9191, https://doi.org/10.1038/s41598-018-27590-z, 2018.

Querol X., Alastuey A., Orio A., Pallares M., Reina F., Dieguez J. J., Mantilla E., Escudero M., Alonso L., Gangoiti G., Millán M.: On the origin of the highest ozone episodes in Spain, Science of the Total Environment, 572, 379-389, 2016.

765 Querol X., Gangoiti G., Mantilla E., Alastuey A., Minguillón M. C., Amato F., Reche C., Viana M., Moreno T.,
766 Karanasiou A., Rivas I., Pérez N., Ripoll A., Brines M., Ealo M., Pandolfi M., Lee H.-K., Eun H.-R., Park Y.-H.,
767 Escudero M., Beddows D., Harrison R.M., Bertrand A., Marchand N., Lyasota A., Codina B., Olid M., Udina M.,
768 Jiménez-Esteve B., Soler M. R., Alonso L., Millán M., Ahn, K.-H.: Phenomenology of high-ozone episodes in NE
769 Spain, Atmospheric Chemistry and Physics, 17, 2817-2838, 2017.

770 Querol, X., Alastuey, A., Gangoiti, G., Perez, N., Lee, H. K., Eun, H. R. Park, Y. Mantilla, E. Escudero, M. Titos,
771 G. Alonso, L. Temime-Roussel, B. March, N. Moreta, J. R. Revuelta, M. A. Salvador, P. Artiñano, B. García
772 dos Santos, S. Anguas, M. Notario, A. Saiz-Lopez, A. Harrison, R. M. Ahn, K.-H.: Phenomenology of summer
773 ozone episodes over the Madrid Metropolitan Area, central Spain, Atmospheric Chemistry and Physics
774 Discussions, 2017, 1–38, https://doi.org/10.5194/acp-2017-1014, 2018.

775 Safieddine, S., Boynard, A., Coheur, P.-F., Hurtmans, D., Pfister, G., Quennehen, B., Thomas, J. L., Raut, J.-C.,
776 Law, K. S., Klimont, Z., Hadji-Lazaro, J., George, M., and Clerbaux, C.: Summertime tropospheric ozone
777 assessment over the Mediterranean region using the thermal infrared IASI/MetOp sounder and the WRF-
778 Chem model, Atmospheric Chemistry and Physics, 14, 10119-10131, 2014.

779 Salvador R., Millán M.M., Mantilla E., and Baldasano J.M.: Mesoscale modelling of atmospheric processes over
780 the western Mediterranean area during summer. International Journal of Environment and Pollution, 8, 513-
781 528.14, 10119-10131, https://doi.org/10.5194/acp-14-10119-2014, 1997.

782 Sen, P. K.: Estimates of regression coefficient based on Kendall's tau, Journal of the American Statistical
783 Association 63(324), 1968.

784 Sicard, P., De Marco, A., Troussier, F., Renou, C., Vas, N., Paoletti, E.: Decrease in surface ozone concentrations
785 at Mediterranean remote sites and increase in the cities, Atmospheric Environment, 79, 705-715, 2013.

786 Solberg S., Hov Ø., Søvde A., Isaksen I.S.A., Coddeville P., De Backer H., Forster C., Orsolini Y., Uhse K.:
787 European surface ozone in the extreme summer 2003, Journal of Geophysical Research, 113, D07307,
788 https://doi.org/10.1029/2007JD009098, 2008.

789 Soriano, C., Baldasano, J.M., Buttler, W.T., Moore, K.: Circulatory patterns of air pollutants within the
790 Barcelona air basin in a summertime situation: lidar and numerical approaches, Boundary-Layer Meteorology
791 98 (1), 33–55, 2001.

792 Stein A.F., Mantilla E., and Millán M.M.: Ozone formation downwind an industrial complex in the western
793 Mediterranean, In: 13th World Clean Air and Environmental Protection, August 22-27. London, U.K., 2004.

794 Stevenson, D. S., Dentener, F. J., Schultz, M. G., Ellingsen, K., van Noije, T. P. C., Wild, O., Zeng, G., Amann, M.,
795 Atherton, C. S., Bell, N., Bergmann, D. J., Bey, I., Butler, T., Cofala, J., Collins, W. J., Derwent, R. G., Doherty, R.
796 M., Drevet, J., Eskes, H. J., Fiore, A. M., Gauss, M., Hauglustaine, D. A., Horowitz, L. W., Isaksen, I. S. A., Krol,
797 M. C., Lamarque, J. F., Lawrence, M. G., Montanaro, V., Muller, J. F., Pitari, G., Prather, M. J., Pyle, J. A., Rast,
798 S., Rodriguez, J. M., Sanderson, M. G., Savage, N. H., Shindell, D. T., Strahan, S. E., Sudo, K., and Szopa, S.:
799 Multimodel ensemble simulations of present-day and near-future tropospheric ozone, Journal of Geophysical
800 Research: Atmospheres, 111, D08301, https://doi.org/10.1029/2005jd006338, 2006.

801 Theil, H.: A rank invariant method of linear and polynomial regression analysis, i, ii, iii, Proceedings of the
802 Koninklijke Nederlandse Akademie Wetenschappen, Series A - Mathematical Sciences 53, 386-392, 521-525,
803 1397-1412, 1950.

804 Toll, I. and Baldasano, J. M.: Modeling of photochemical air pollution in the Barcelona area with highly
805 disaggregated anthropogenic and biogenic emissions, Atmospheric Environment, 34(19), 3069–3084,
806 https://doi.org/10.1016/S1352-2310(99)00498-7, 2000.

UNECE: Hemispheric transport of air pollution 2010, Part A: ozone and particulate matter, Air pollution studies, 17, UNECE, LRTAP, Task Force on Hemispheric Transport of Pollutants HTAP 2010: Part A. Ozone and Particulate Matter, 278 pp, ECE/EB.AIR/100, ISBN 978-92-1-117043-6 http://www.htap.org/publications/2010_report/2010_Final_Report/HTAP%202010%20Part%20A%201104 07.pdf, last access: 3 November 2017, 2010.

Valverde V., Pay M.T., Baldasano J.M.: Ozone attributed to Madrid and Barcelona on-road transport emissions: Characterization of plume dynamics over the Iberian Peninsula, Science of the Total Environment, 543, 670–682, 2016.

Vautard, R., Beekmann, M., Desplat, J., Hodzic, A., & Morel, S.: Air quality in Europe during the summer of 2003 as a prototype of air quality in a warmer climate, Comptes Rendus - Geoscience, 339(11–12), 747–763, https://doi.org/10.1016/j.crte.2007.08.003, 2007.

WHO: Air Quality Guidelines: Global Update 2005. Particulate matter, ozone, nitrogen dioxide and sulfur dioxide, World Health Organisation, Copenhagen, ISBN 92 890 2192 6, 484 pp., http://www.euro.who.int/__data/assets/pdf_file/0005/78638/E90038.pdf, last access: 23 November 2017, 2006.

WHO Regional Office for Europe: Review of evidence on health aspects of air pollution—REVIHAAP project: technical report, WHO Regional Office for Europe, Copenhagen 302 pp., http://www.euro.who.int/__data/assets/pdf_file/0004/193108/REVIHAAP-Final-technical-report-final-version.pdf?ua=1, last access: 23 January 2018, 2013a.

WHO Regional Office for Europe: Health Risks of Air Pollution in Europe—HRAPIE Project: Recommendations for Concentration-Response Functions for Cost–Benefit Analysis of Particulate Matter, Ozone and Nitrogen Dioxide, Copenhagen, 65 pp., http://www.euro.who.int/__data/assets/pdf_file/0017/234026/e96933.pdf?ua=1, last access: 23 January 2018, 2013b.

Young, P. J., Archibald, A. T., Bowman, K. W., Lamarque, J.-F., Naik, V., Stevenson, D. S., Tilmes, S., Voulgarakis, A., Wild, O., Bergmann, D., Cameron-Smith, P., Cionni, I., Collins, W. J., Dalsøren, S. B., Doherty, R. M., Eyring, V., Faluvegi, G., Horowitz, L. W., Josse, B., Lee, Y. H., MacKenzie, I. A., Nagashima, T., Plummer, D. A., Righi, M., Rumbold, S. T., Skeie, R. B., Shindell, D. T., Strode, S. A., Sudo, K., Szopa, S., and Zeng, G.: Preindustrial to end 21st century projections of tropospheric ozone from the Atmospheric Chemistry and Climate Model Intercomparison Project (ACCMIP), Atmospheric Chemistry and Physics, 13, 2063 – 2090, https://doi.org/10.5194/acp-13-2063-2013, 2013.

FIGURE CAPTIONS

Figure 1. Location and main topographic features of the area of study.

Figure 2. Location (left) and main characteristics (right) of the selected air quality monitoring sites (S–N axis: green squares on the map and shaded gray on the table, rest of stations: white squares) and meteorological/solar radiation stations (red circles) selected for this study. Types of air quality monitoring sites are urban (traffic or background: UT, UB), suburban (traffic, industrial or background: SUT, SUI, SUB) and rural (background or industrial: RB, RI). PLR (Palau Reial air quality monitoring site) and BCN (Barcelona) meteorological and solar radiation sites are closely located.

Figure 3. Spatial variability of mean June–August O_3 (a) and O_x (b) concentrations from 12:00 to 19:00 h observed in selected air quality monitoring sites. Data from Ciutadella (CTL), Palau Reial (PLR), Montcada (MON), Granollers (GRA), Montseny (MSY), Tona (TON), Vic (VIC), Manlleu (MAN), Pardines (PAR), Montsec (MSC), Begur (BEG), Bellver de Cerdanya (BdC), Berga (BER), Agullana (AGU), Santa Pau (STP), Mataró (MAT), Manresa (MNR), Ponts (PON), Sort (SOR), Juneda (JUN), La Sénia (LSE), Constantí (CON), Gandesa (GAN), Vilanova i la Geltrú (VGe) and Alcover (ALC) air quality monitoring stations.

Figure 4. Results of the time trend assessment carried out for annual season averages (April–September) of NO (a), NO_2 (b), O_3 (c & d) and O_x (e) levels using the Theil–Sen statistical estimator shown graphically. Only shown the trends with statistical significance. (d) Numerical results; the symbols shown for the p-values related to how statistically significant the trend estimate is: $p < 0.001$ = *** (highest statistical significance), $p < 0.01$ = ** (mid), $p < 0.05$ = * (moderate), $p < 0.1$ = + (low). No symbol means lack of significant trend. Units are µg m^{-3}. Shaded air quality monitoring sites belong to the S–N axis. Types of air quality monitoring sites are urban (traffic or background: UT, UB), suburban (traffic, industrial or background: SUT, SUI, SUB) and rural (background: RB). Data from AQ stations with at least 10 years of valid data within the period.

Figure 5. (a) Annual average traffic entering Barcelona City during weekdays (weekends not considered) during 2005–2016 versus GHG emissions (attributed to industry and power generation sectors) in Catalonia during 2005–2016. (b) Annual NO_x measured at CTL (Ciutadella) and MON (Montcada) air quality monitoring sites versus annual OMI-NASA's measured background NO_2 during 2005–2017.

Figure 6. Monthly hourly average concentrations of O_3 (a) and O_X (b) along the S–N axis during 2005–2017. Data from Ciutadella (CTL), Montcada (MON), Granollers (GRA), Montseny (MSY), Tona (TON), Vic (VIC), Manlleu (MAN) and Pardines (PAR) air quality monitoring stations.

Figure 7. Monthly weekday average concentrations of O_3 concentrations calculated between 12:00 and 19:00 h along the S–N axis during 2005–2017. Data from Ciutadella (CTL), Montcada (MON), Granollers (GRA), Montseny (MSY), Tona (TON), Vic (VIC), Manlleu (MAN) and Pardines (PAR) air quality monitoring stations.

Figure 8. Weekday (W) (Monday to Friday in the BMA and Tuesday to Friday in the Vic Plain) to Weekend (WE) pollutant concentrations (O_3, NO and NO_2) measured at AQ sites and background NO_2 (remote sensing OMI) for June to August, per year along the period 2005−2017. O_3 concentrations (top plot) are averaged from 12:00 to 19:00 h LT hourly concentrations, and NO and NO_2 concentrations are calculated from daily averages, including OMI-NO_2. Each short line depicts the increasing or decreasing tendency of weekday concentrations (left side of each short line) with respect to weekend levels (right side of the short line). Thus, a horizontal line would represent same pollutant levels along the week (concentration in W = concentration in WE). We consider BMA AQ sites: CTL, MON and GRA and Vic Plain AQ sites: TON and MAN. The continuous lines show the percentage of variation of pollutant levels during weekends with respect to weekdays: increasing (>0) or decreasing (<0) i.e. a quantification of the inclination of each short line.

Figure 9. (a) July O_3 and (b) O_x daily cycles plotted from mean hourly concentrations measured in air quality monitoring sites located along the S–N axis during 2005–2017. The black arrows point to the O_3 and O_x maxima

time of the day. Data from Ciutadella (CTL), Montcada (MON), Granollers (GRA), Montseny (MSY), Tona (TON), Vic (VIC), Manlleu (MAN) and Pardines (PAR) air quality monitoring stations.

Figure 10**.** For the period 2005–2017, trends of the EHITs measured by air quality monitoring stations along the S–N axis (a) Annual trends of the EHITs, average temperatures measured in Vic (Gurb) (July during 13:00 to 16:00 h), background NO_2 measured by OMI-NASA (June to August) and average solar radiation measured at Girona and Barcelona (June to August). (b) Monthly patterns of the EHITs, average temperatures measured in Vic, background NO_2 measured by OMI and solar radiation measured at Girona and Barcelona. (c) Weekly patterns of the EHITs and background NO_2 measured by OMI. (d) Hourly patterns of the EHITs. Despite the incomplete data availability in MAN 2005, almost 20 EHITs were recorded. AQ data from Ciutadella (CTL), Montcada (MON), Granollers (GRA), Montseny (MSY), Tona (TON), Vic (VIC), Manlleu (MAN) and Pardines (PAR) monitoring stations.

Figure 11. Average hourly O_3 concentrations for all days with EHIT records and those without for Tona (TON), Vic (VIC), Manlleu (MAN) and Pardines (PAR) air quality monitoring stations, (left top) as well as for the NO_2 levels at TON (left bottom). Average hourly increments of O_3 concentrations for all days with and without EHIT records (right); in all cases for June–August 2005–2017.

Figure 12. Idealized two-dimensional section of O_3 circulations in the coastal region of Barcelona to the Pre-Pyrenees on a typical summer day (upper) and night (bottom). The gray shaded shape represents a topographic profile south to north direction, from the Mediterranean Sea to the south slopes of the Pre-Pyrenean Ranges (i.e., along the S–N axis). The colored dots and abbreviations depict the air quality monitoring stations located along the S–N axis: Ciutadella (CTL), Montcada (MON), Granollers (GRA), Montseny (MSY), Tona (TON), Vic (VIC), Manlleu (MAN) and Pardines (PAR). Modified and adapted to the S–N axis from Millán et al. (1997, 2000), Querol et al. (2017, 2018).

Figure 13. Daily average background NO_2 levels in Western Europe (top) and Catalonia (bottom), July 2005–2017 in two different scenarios. (Left) P25: days when the maximum daily 8-h mean O_3 concentrations in the Vic Plain are below the percentile 25 (<105 μg m^{-3}) and (right) P75: same but concentrations being above the percentile 75 (>139.5 μg m^{-3}).

Figure 14. Box plots of O_x measured in TON and MAN (12:00 to 19:00h) per weekday June and July 2005–2017 for those days with $\delta O_{x\ TON-CTL} > 0$ (n = 545 for TON and n = 479 for MAN of valid data). Each box represents the central half of the data between the lower quartile (P25) and the upper quartile (P75). The lines across the box displays the median values. The whiskers that extend from the bottom and the top of the box represent the extent of the main body of data. The outliers are represented by black points.

FIGURES

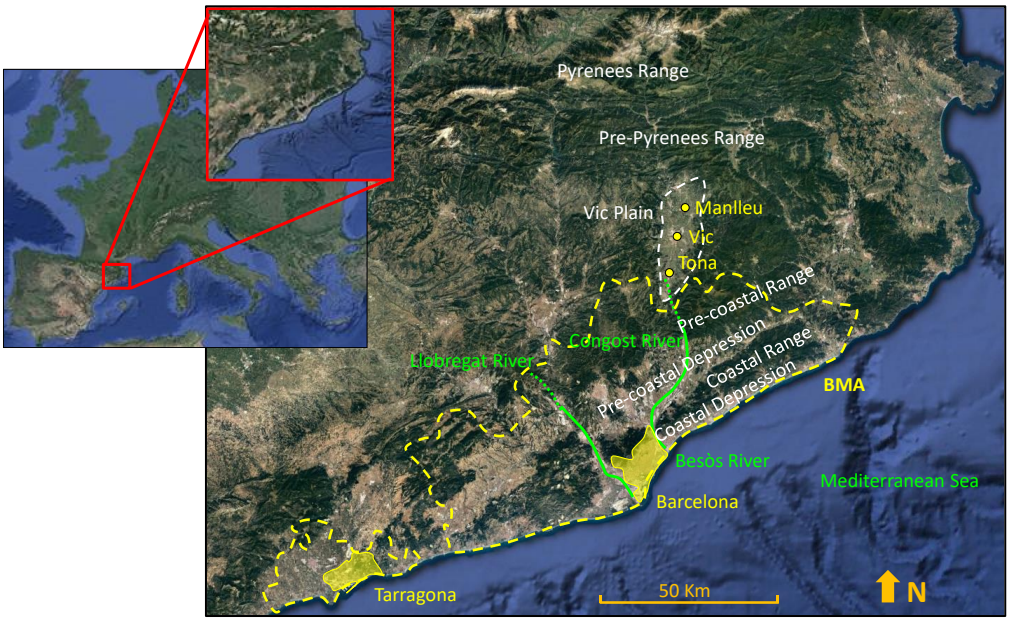

Figure 1

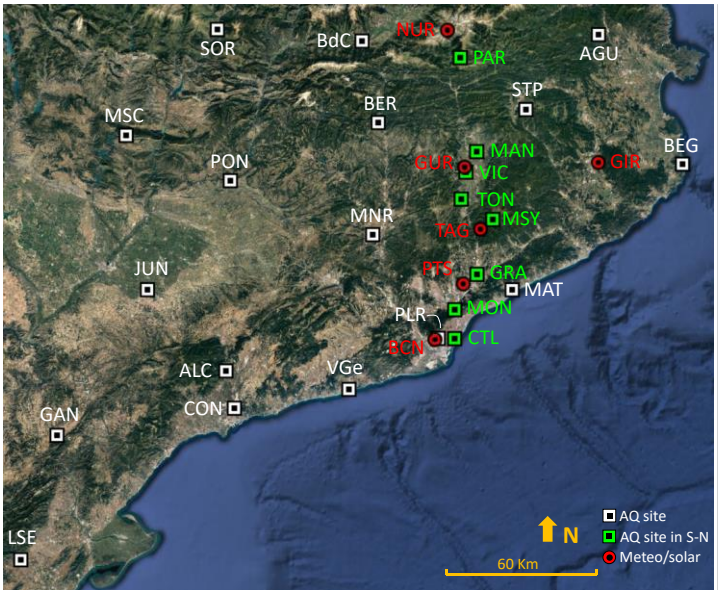

AQ site	Code	Type	Elevation (m.a.s.l.)	Latitude (deg.)	Longitude (deg.)
Ciutadella	CTL	UB	7	41.39	2.10
Montcada	MON	SUT	34	41.48	2.19
Granollers	GRA	UT	133	41.60	2.29
Montseny	MSY	RB	693	41.78	2.36
Tona	TON	RB	620	41.85	2.22
Vic	VIC	SUB	498	41.94	2.24
Manlleu	MAN	SUB	460	42.00	2.29
Pardines	PAR	RB	1226	42.31	2.21
Palau Reial	PLR	UB	81	41.39	2.12
Montsec	MSC	RB	1570	42.05	0.73
Begur	BEG	RB	200	41.96	3.21
Bellver de Cerdanya	BdC	RB	1060	42.37	1.78
Berga	BER	SUB	661	42.10	1.85
Agullana	AGU	RB	214	42.39	2.84
Santa Pau	STP	RB	496	42.14	2.51
Mataró	MAT	UB	40	41.55	2.44
Manresa	MNR	UT	238	41.73	1.83
Ponts	PON	RB	370	41.91	1.19
Sort	SOR	RB	692	42.41	1.13
Juneda	JUN	RB	255	41.54	0.83
La Sénia	LSE	RB	428	40.64	0.29
Constantí	CON	SUI	56	41.15	1.22
Gandesa	GAN	RB	368	41.06	0.44
Vilanova i la Geltrú	VGe	SUT	12	41.23	1.72
Alcover	ALC	RI	238	41.28	1.18

Meteo/Solar radiation site	Code	Anemom height (m)	Elevation (m.a.s.l.)	Latitude (deg.)	Longitude (deg.)
Fac. Física UB (Bcn)	BCN	-	70	41.38	2.12
Parets del Vallès	PTS	10	123	41.57	2.23
Montseny	TAG	2	1030	41.75	2.30
Gurb	GUR	2	509	41.95	2.23
Nuria	NUR	10	1971	42.40	2.16
Barcelona	BCN	(solar)	125	41.38	2.10
Girona	GIR	(solar)	115	41.97	2.83

Figure 2

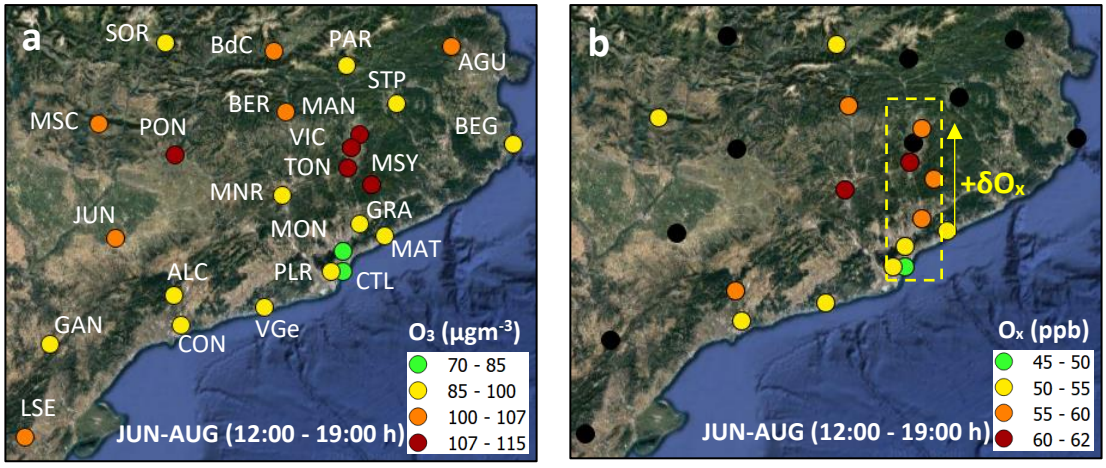

947 Figure 3

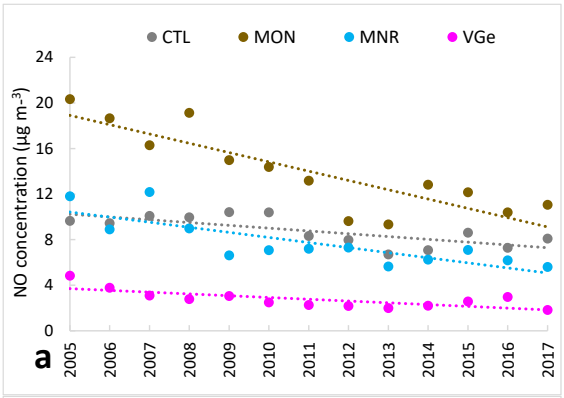

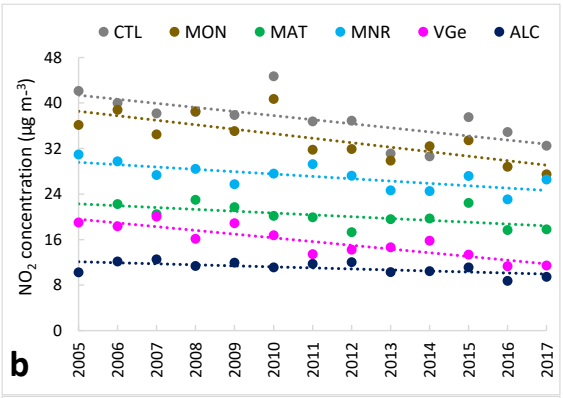

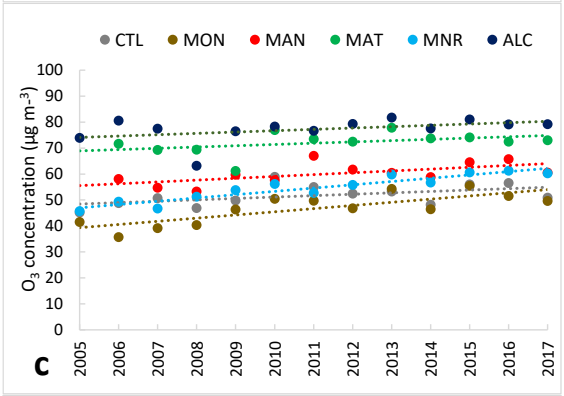

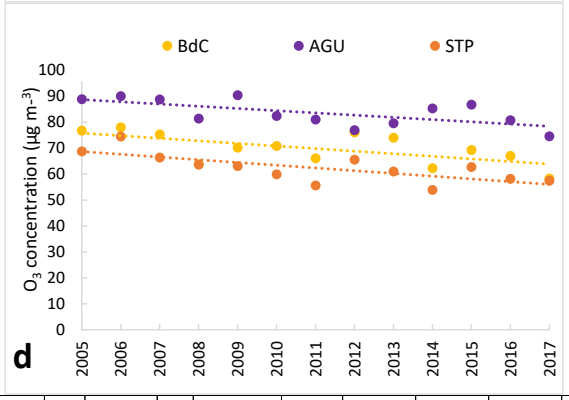

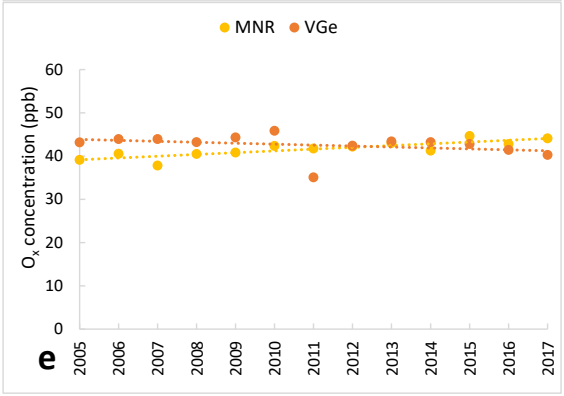

APR-SEP	site	type	period	years	initial concentration	%/year	%/year min	%/year max	%/period	p-Value
NO	CTL	UB	2005-2017	13	9.7	-2.2	-3.7	-1.1	-28.8	*
	MON	SUT	2005-2017	13	20.3	-4.3	-6.2	-3.3	-56.5	***
	MNR	UT	2005-2017	13	11.8	-3.8	-5.9	-1.6	-49.0	**
	VGe	SUT	2005-2017	13	4.8	-4.4	-6.5	-0.4	-57.2	*
NO_2	CTL	UB	2005-2017	13	42.1	-1.6	-2.8	-0.9	-20.6	***
	MON	SUT	2005-2017	13	36.2	-2.0	-3.0	-1.2	-25.5	**
	MAN	SUB	2006-2017	12	15.7	-1.3	-2.2	-0.4	-15.8	*
	MAT	UB	2006-2017	12	22.2	-1.7	-2.5	-0.4	-19.9	*
	MNR	UT	2005-2017	13	31.0	-1.4	-2.3	-0.4	-18.0	**
	VGe	SUT	2005-2017	13	19.0	-3.3	-4.3	-2.5	-43.3	**
	ALC	SUI	2005-2017	13	10.3	-1.6	-2.5	0.0	-21.4	+
O_3	CTL	UB	2005-2017	13	45.1	1.4	-0.6	2.4	17.8	+
	MON	SUT	2005-2017	13	41.5	3.2	1.3	6.0	42.1	**
	MAN	SUB	2006-2017	12	58.0	1.3	0.0	2.5	15.9	*
	BdC	RB	2005-2017	13	76.7	-1.6	-2.1	0.0	-20.5	+
	AGU	RB	2005-2017	13	88.9	-1.1	-1.6	-0.2	-13.8	*
	STP	RB	2005-2017	13	68.7	-1.4	-2.6	-0.8	-18.0	***
	MAT	UB	2006-2017	12	71.6	0.4	-0.3	1.3	4.9	+
	MNR	UT	2005-2017	13	45.6	2.6	1.8	3.5	33.7	***
	ALC	SUI	2005-2017	13	73.9	0.5	0.0	1.5	6.8	*
O_x	MNR	UT	2005-2017	13	39.1	1.1	0.6	1.5	14.2	***
	VGe	SUT	2005-2017	13	43.1	-0.5	-0.9	0.1	-6.5	+

948 Figure 4

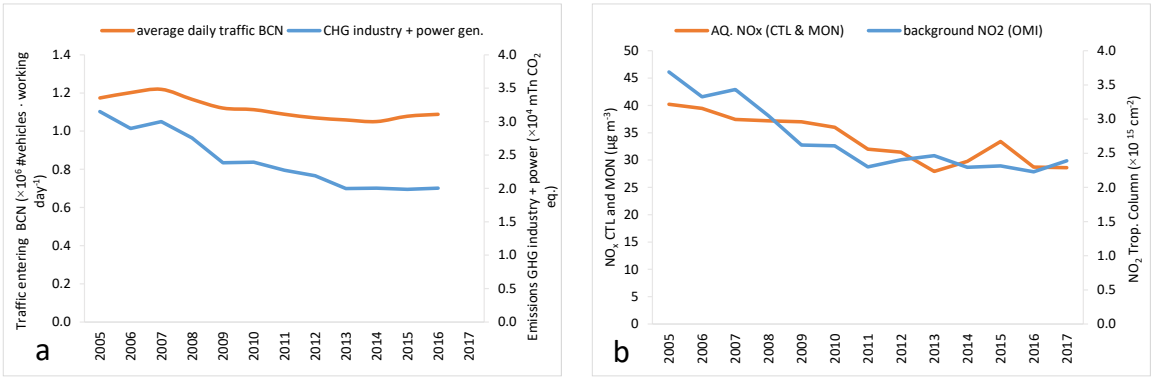

949 Figure 5

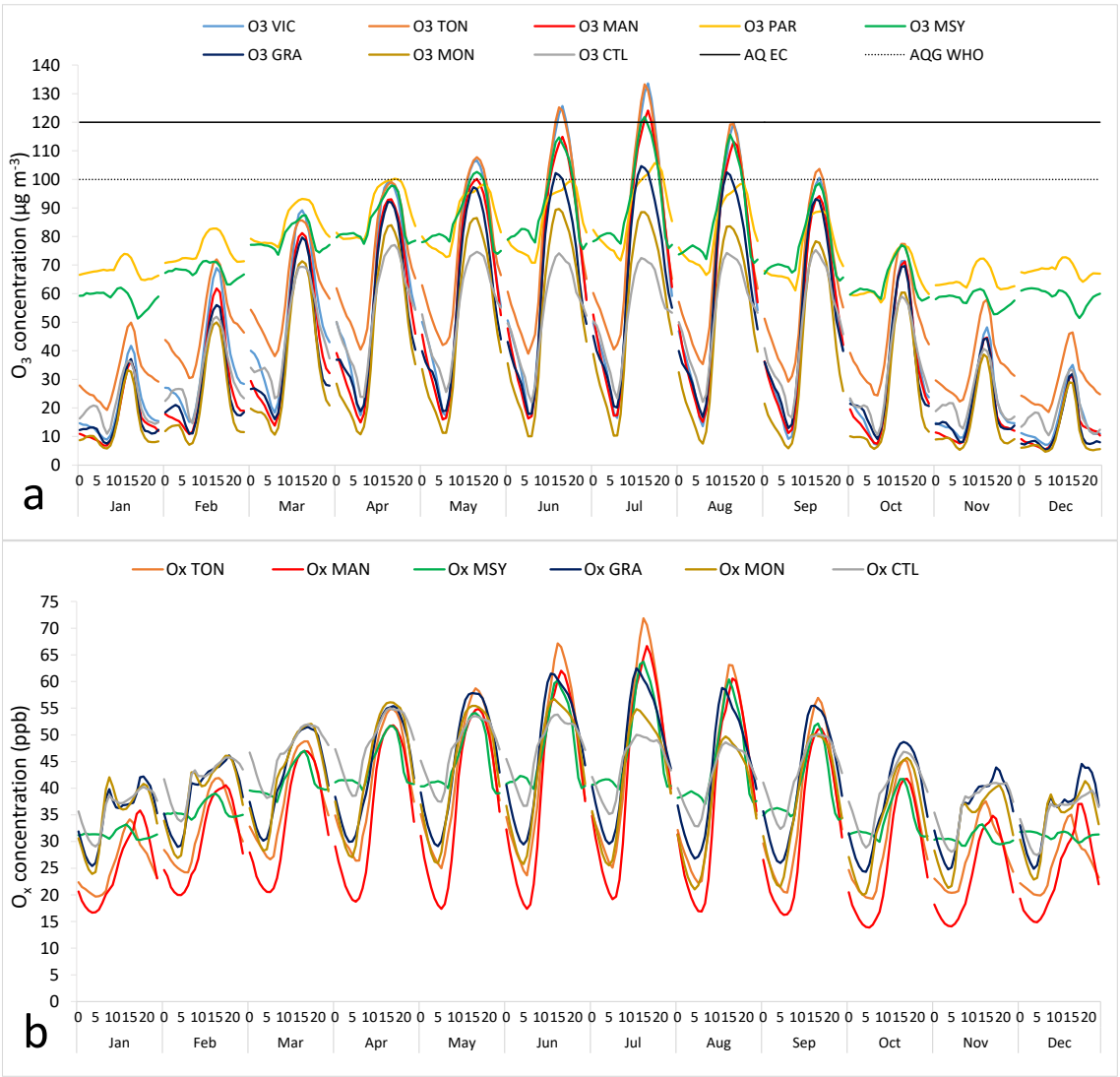

950

951

952 Figure 6

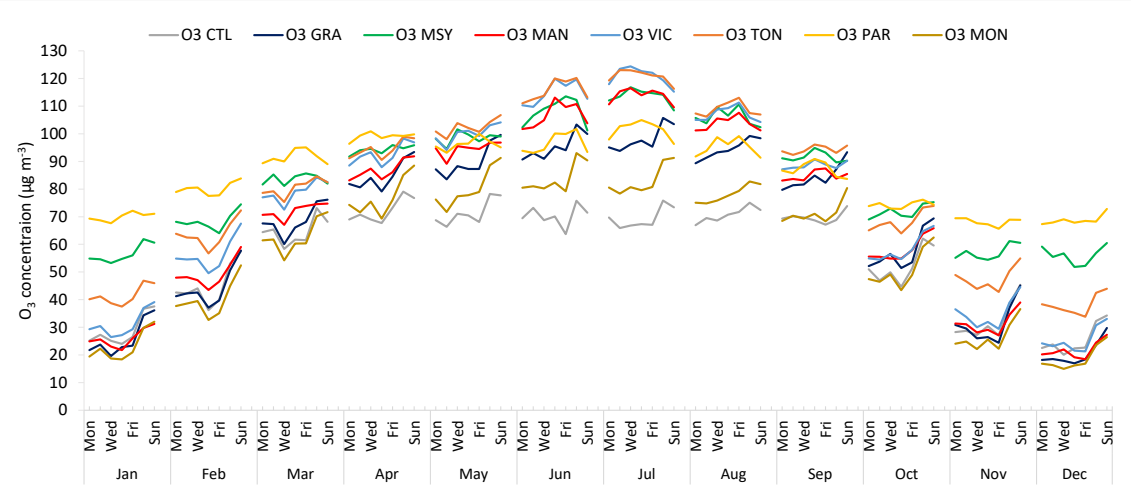

953

954 Figure 7

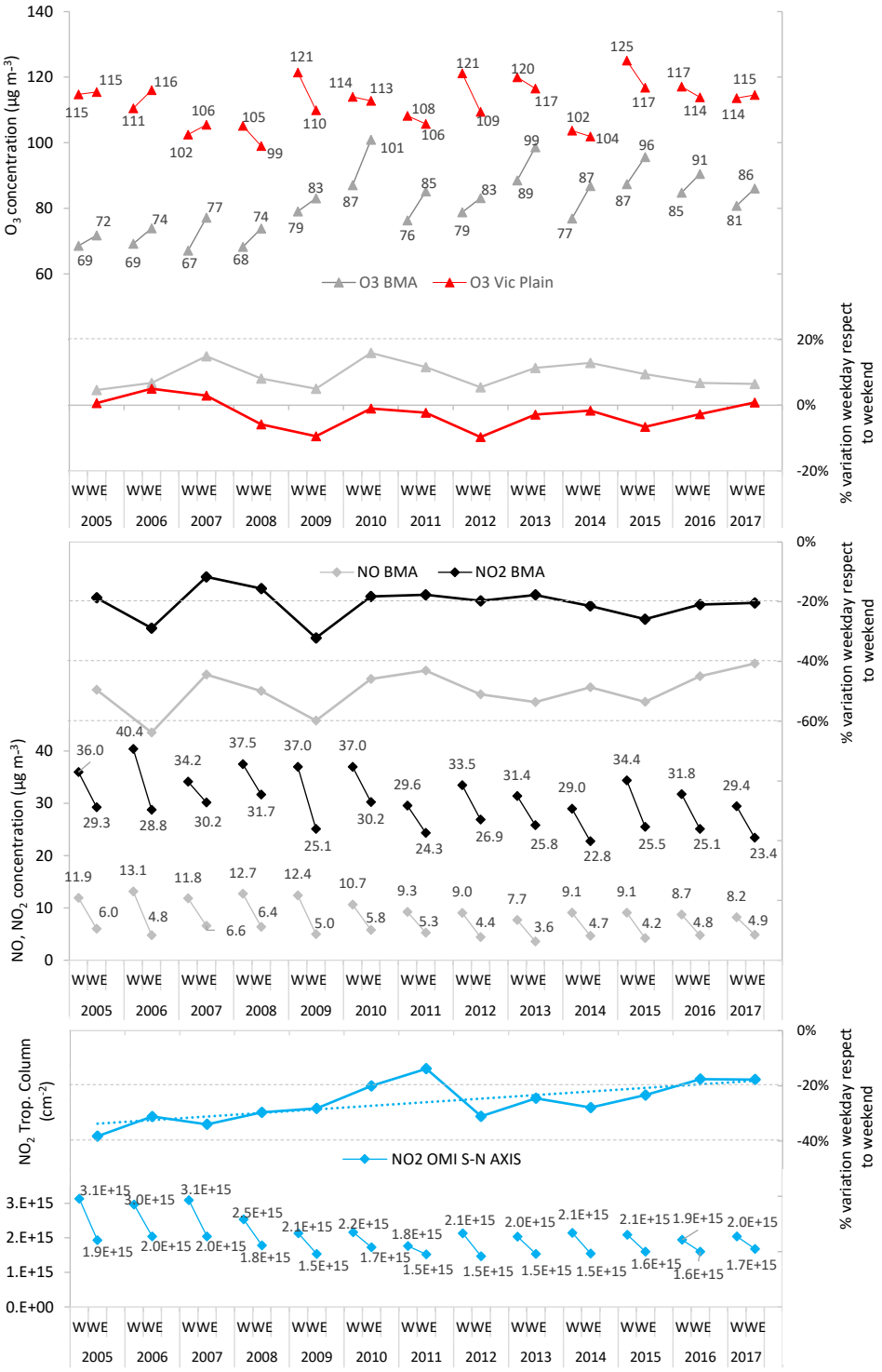

955

956 Figure 8

957

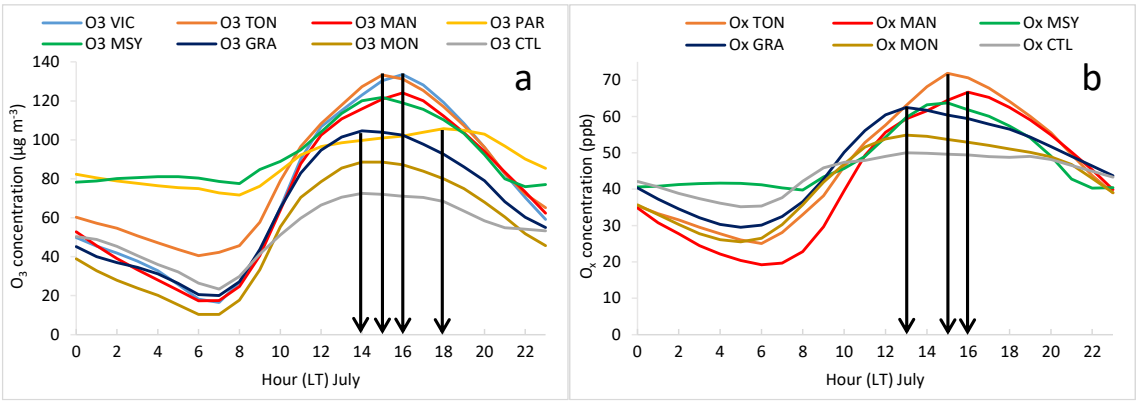

958 Figure 9

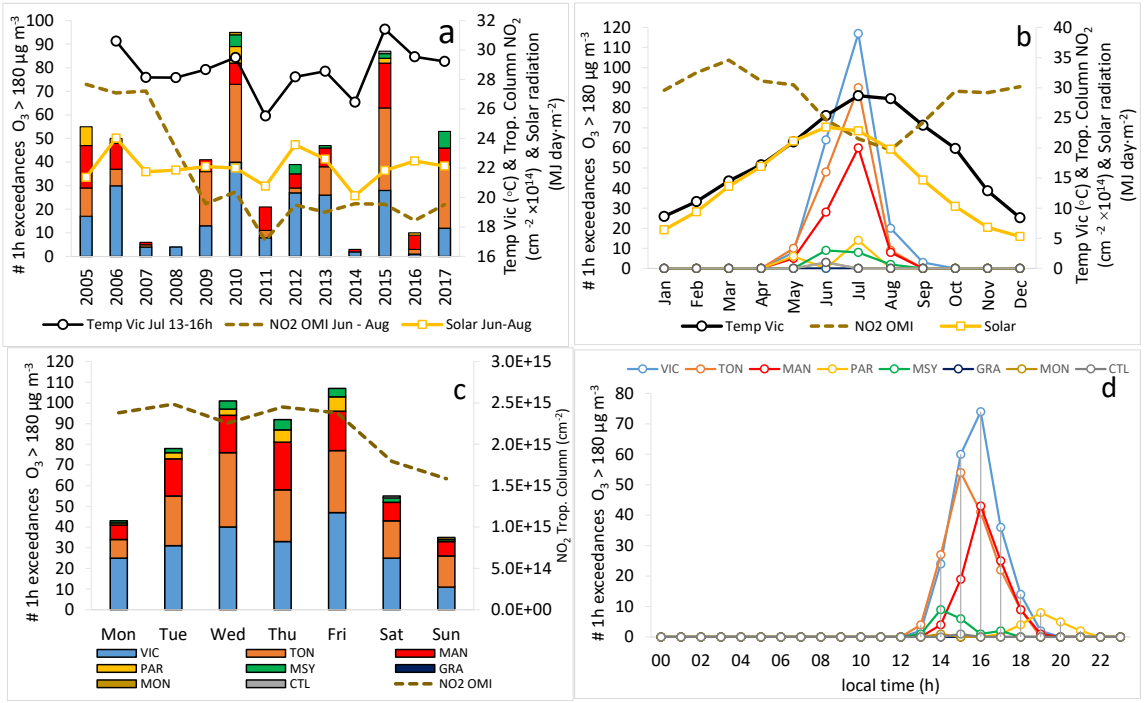

959 Figure 10

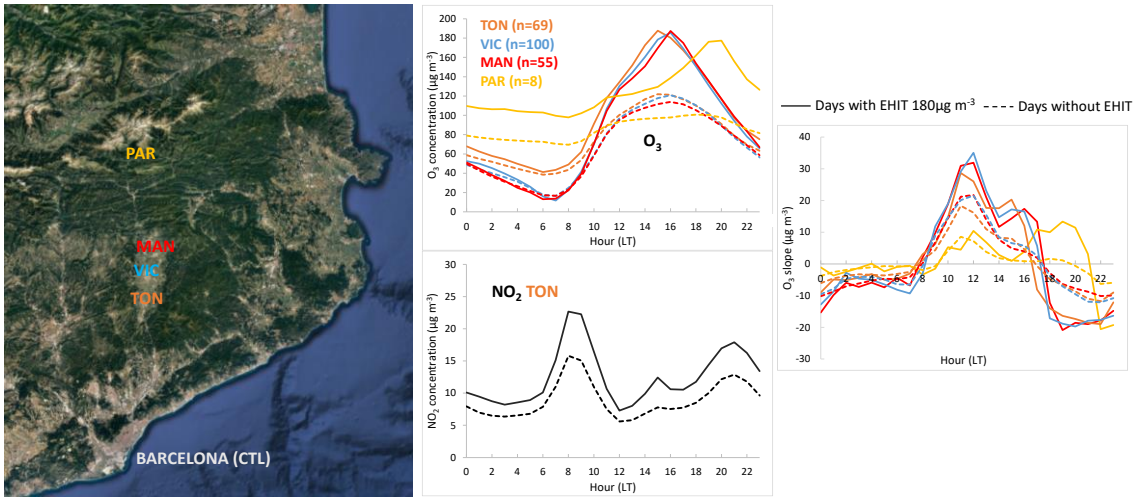

960

961 Figure 11

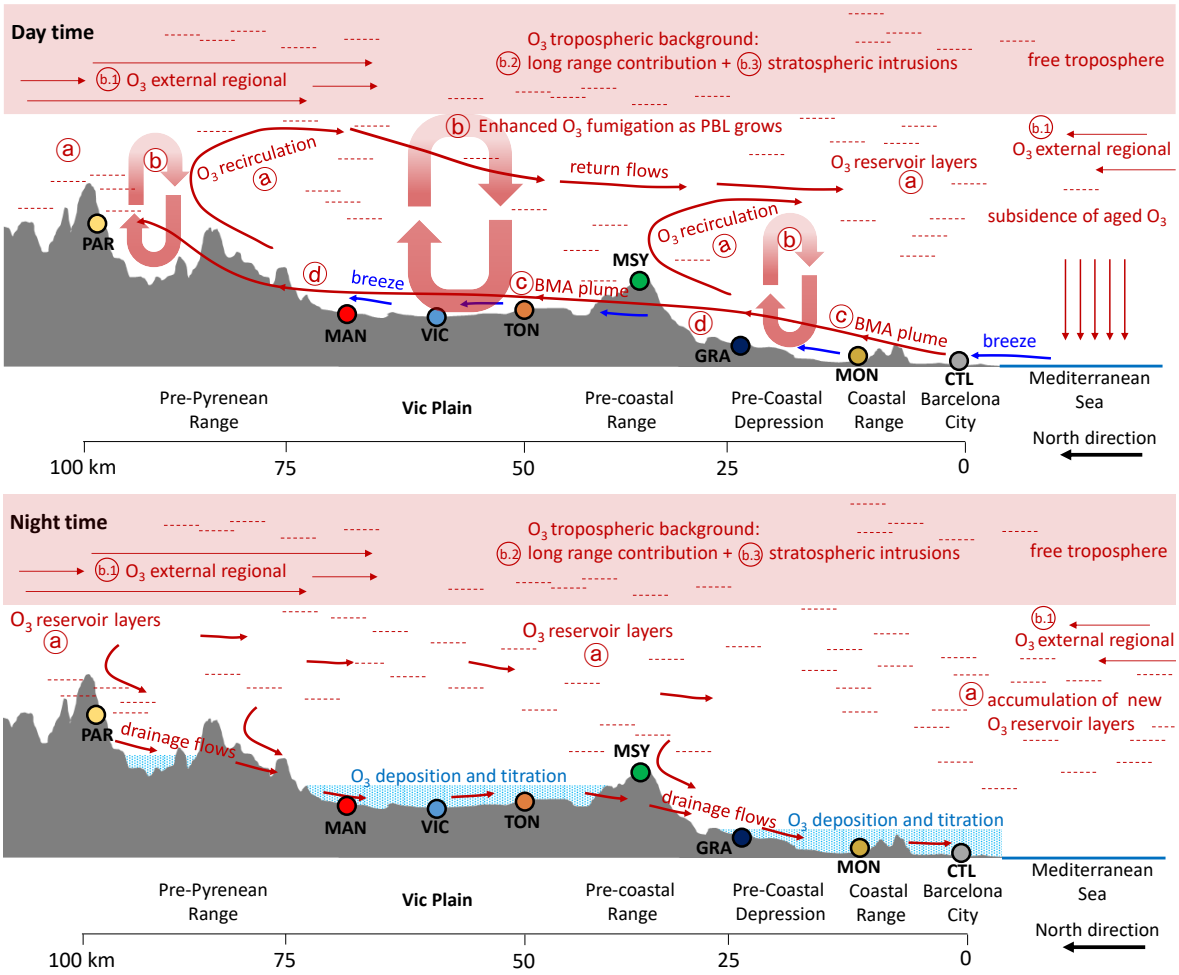

962

963

964 Figure 12

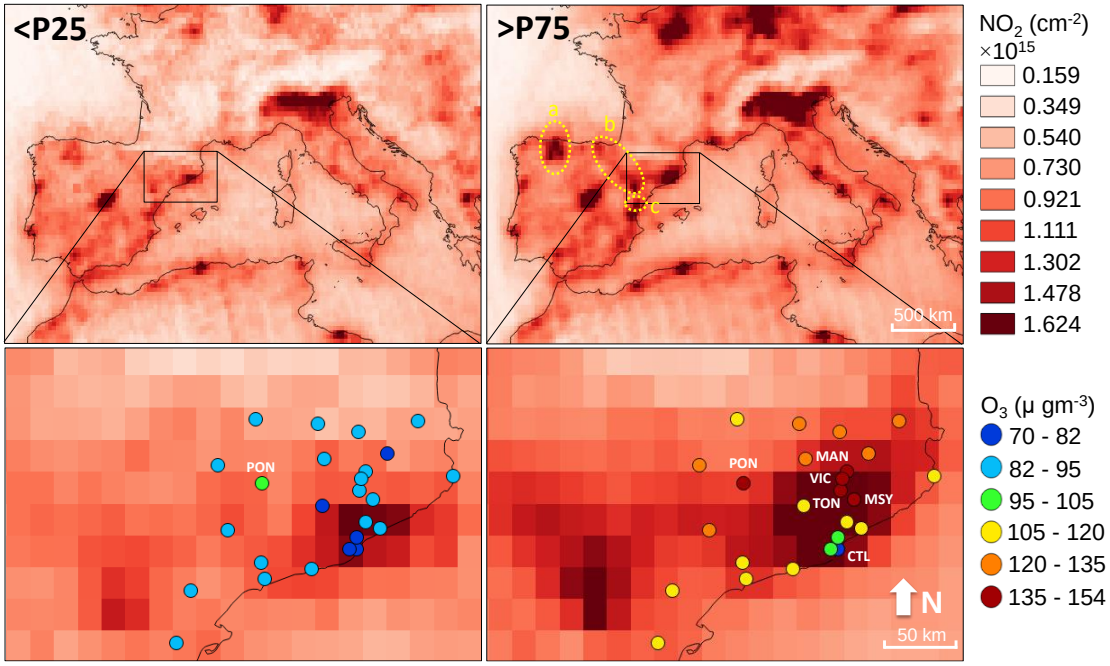

965

966 Figure 13

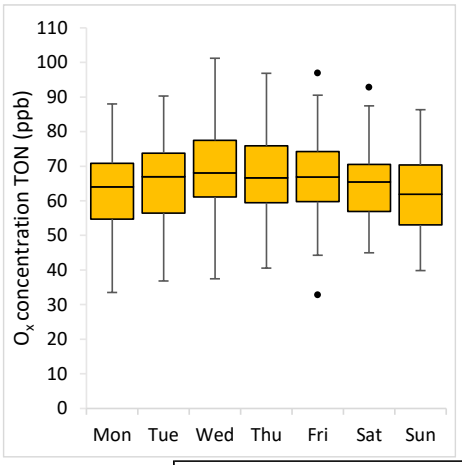

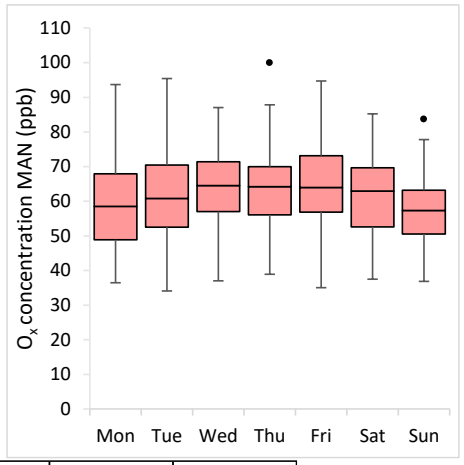

Avg. O_x June & July 12:00 - 19:00 LT (2005-2017)	TON	MAN
maximum percentile 75 (ppb)	77.5 (Wed.)	73.1 (Fri.)
minimum percentile 25 (ppb)	53.0 (Sun.)	48.8 (Mon.)
max. intra week diff: max p.75 - min p.25 (ppb)	24.5 (-32%)	24.3 (-33%)
max average (ppb)	68.0 (Wed.)	64.6 (Wed.)
min average (ppb)	61.5 (Sun.)	56.8 (Sun.)
intra week diff: max avg.- min avg. (ppb)	6.5 (-10%)	7.7 (-12%)

967 Figure 14

968